A THESIS SUBMITTED TO
THE GRADUATE SCHOOL OF NATURAL AND APPLIED SCIENCES
OF ÇANKIRI KARATEKİN UNIVERSITY

INVESTIGATION OF THERMODYNAMIC PROPERTIES OF FAVIPIRAVIR AND RIBAVIRIN MOLECULAR STRUCTURES USED IN THE TREATMENT OF COVID-19 AND THEIR INTERACTION WITH DNA BASES BY DFT

IN PARTIAL FULFILLMENT OF THE REQUIREMENTS
FOR
THE DEGREE OF MASTER OF SCIENCE
IN
PHYSICS

BY

MUSTAFA FAWZI DAWOOD ALOBAIDI

ÇANKIRI

2023

INVESTIGATION OF THERMODYNAMIC PROPERTIES OF FAVIPIRAVIR AND RIBAVIRIN MOLECULAR STRUCTURES USED IN THE TREATMENT OF COVID-19 AND THEIR INTERACTION WITH DNA BASES BY DFT

By Mustafa Fawzi Dawood ALOBAIDI

February 2023

We certify that we have read this thesis and that in our opinion it is fully adequate, in scope and in quality, as a thesis for the degree of Master of Science

Advisor **:** Prof. Dr. Çiğdem YÜKSEKTEPE ATAOL

Examining Committee Members:

Chairman **:** Prof. Dr. Çiğdem YÜKSEKTEPE ATAOL
Physics
Çankırı Karatekin University

Member **:** Prof. Dr. Hamit ALYAR
Physics
Çankırı Karatekin University

Member **:** Assoc. Prof. Dr. Ayşin ZÜLFİKAROĞLU
Chemistry
Amasya University

Approved for the Graduate School of Natural and Applied Sciences

Prof. Dr. İbrahim ÇİFTÇİ
Director of Graduate School

I hereby declare that all information in this document has been obtained and presented in accordance with academic rules and ethical conduct. I also declare that, as required by these rules and conduct, I have fully cited and referenced all material and results that are not original to this work.

Mustafa Fawzi Dawood ALOBAIDI

ABSTRACT

INVESTIGATION OF THERMODYNAMIC PROPERTIES OF FAVIPIRAVIR AND RIBAVIRIN MOLECULAR STRUCTURES USED IN THE TREATMENT OF COVID-19 AND THEIR INTERACTION WITH DNA BASES BY DFT

Mustafa Fawzi Dawood ALOBAIDI

Master of Science in Physics

Advisor: Prof. Dr. Çiğdem YÜKSEKTEPE ATAOL

February 2023

Different properties of the molecular structures of favipiravir and ribavirin, which are used in the treatment of SARS-CoV-2 and also needed in the treatment of coronavirus disease (COVID-19) in recent years, have been investigated using Density Functional Theory (DFT) B3LYP/6-311G(d, p) and 6-311+G(d, p) methods. The geometrical optimization of the molecular structures of favipiravir and ribavirin was made in the ground state, gas, and water solvent environments, the bond parameters were obtained and the theoretical results were compared with the values in the literature. By obtaining molecular orbital energy values from energy calculations, global reactivity parameters such as electron affinity, electronegativity, chemical potential, chemical hardness, softness, and electrophilicity index were obtained for both environments. The interactions between adenine, guanine, cytosine, and thymine DNA bases and the molecular structures of favipiravir and ribavirin were investigated in water with the help of two parameters such as ΔN (charge transfer) and ECT (electrophilicity-based charge transfer) using global reactivity values. By using the optimized molecular structures of favipiravir and ribavirin, ground state frequency calculations were made for both environments, and thermodynamic properties of molecular structures such as entropy, enthalpy, heat capacity, zero point vibration energy, and Gibbs free energy were investigated.

2023, 56 pages

Keywords: Favipiravir, Ribavirin, COVID-19, DNA bases, DFT

ÖZET

COVID-19 TEDAVİSİNDE KULLANILAN FAVİPİRAVİR VE RİBAVİRİN MOLEKÜLER YAPILARININ TERMODİNAMİK ÖZELLİKLERİNİN VE DNA BAZLARI İLE ETKİLEŞİMİNİN DFT İLE ARAŞTIRILMASI

Mustafa Fawzi Dawood ALOBAIDI

Fizik, Yüksek Lisans

Tez Danışmanı: Prof. Dr. Çiğdem YÜKSEKTEPE ATAOL

Şubat 2023

SARS-CoV-2 tedavisinde kullanılan ve ayrıca son yıllarda insanların koranavirüs hastalığı (COVID-19) tedavisinde ihtiyaç duyduğu ilaçlardan favipiravirin ve ribavirinin moleküler yapılarının farklı özellikleri Yoğunluk Fonksiyonel Teorisi (YFT) B3LYP/6-311G(d, p) ve 6-311+G(d, p) yöntemleri kullanılarak araştırılmıştır. Favipiravir ve ribavirinin moleküler yapılarının geometrik optimizasyonu taban durumda, gaz ve su çözücü ortamlarında yapılmış, bağ parametreleri elde edilmiş ve bulunan teorik sonuçlar literatürdeki değerler ile karşılaştırılmıştır. Enerji hesaplamalarından, moleküler orbital enerji değerleri elde edilerek, her iki ortam için, elektron ilgisi, elektronegatiflik, kimyasal potansiyel, kimyasal sertlik, yumuşaklık, elektrofilisiti indeks gibi küresel reaktivite parametreleri elde edilmiştir. Küresel reaktivite değerleri kullanılarak ΔN (yük transfer) ve ECT (elektrofilisiti temelli yük transfer) gibi iki parametre yardımıyla adenin, guanin, sitozin ve timin DNA bazları ile favipiravir ve ribavirin moleküler yapıları arasındaki etkileşimler su ortamında araştırılmıştır. Optimize edilen favipiravin ve ribavirin moleküler yapıları kullanılarak her iki ortam için taban durumda frekans hesabı yapılmış ve moleküler yapıların entropi, entalpi, ısı sığası, sıfır nokta titreşim enerjisi ve Gibbs serbest enerji gibi termodinamik özellikleri araştırılmıştır.

2023, 56 sayfa

Anahtar Kelimeler: Favipiravir, Ribavirin, COVID-19, DNA bazları, DFT

PREFACE AND ACKNOWLEDGEMENTS

I would like to thank my thesis advisor, Prof. Dr. Çiğdem YÜKSEKTEPE ATAOL, for her patience, guidance and understanding.

Mustafa Fawzi Dawood ALOBAIDI

Çankırı-2023

CONTENTS

LIST OF SYMBOLS

$\hat{H}$	Hamiltonian operator
+	Plus
<	Less than
>	Greater than
C	Heat capacity
E_{xc}	Exchange-correlation energy
H	Enthalpy
J	Joule
K	Kelvin
kg	Kilogram
S	Entropy
S	Global softness
ΔE	Energy gap
ΔN	Charge transfer
η	Chemical hardness
μ	Chemical potential
χ	Electronegativity
Ψ	Wavefunction
ω	Electrophilicity index

LIST OF ABBREVIATIONS

ARDS	Acute respiratory distress syndrome
COVID-19	Coronavirus disease
DFT	Density functional theory
DNA	Deoxyribonucleic acid
ECT	Electrophilicity-based charge transfer
HIV	Human immunodeficiency virus
HOMO	Highest occupied molecular orbital
LUMO	Lowest unoccupied molecular orbital
MEP	Molecular electrostatic potential
mtDNA	Mitochondrial DNA
RdRp	RNA-dependent RNA polymerase
RG	Runge-gross
RNA	Ribonucleic acid
ZPVE	Zero-point vibrational energy

LIST OF FIGURES

LIST OF TABLES

1. INTRODUCTION

Earth has faced a global health crisis as a result of this epidemic scenario produced due to the illness COVID-19, It is brought on by SARS-CoV2, a virus belonging to the coronavirus household (Gorbalenya *et al.* 2020). Which has been exposed to mankind for the past two years, high fever, severe respiratory issues, polypnea, weakness, myalgia, and coughs are all common symptoms of COVID-19 infections, the illness as well leads to acute respiratory distress syndrome (ARDS) and dying (Aytür *et al.* 2020). The likelihood of major symptoms and mortality in COVID-19 patients will rise with 60 age and older, it is undeniable, and in those with additional serious medical conditions such as extreme fatness, diabetes, heart, lung, renal, or liver problems (Wang *et al.* 2020). Beginning with COVID-19's initial phase, both researchers and medical professionals operating continuously to seek out an economical result within the kind of medicine and immunizing agent versus sickness. Many reconfigured and novel medicines, plasma-based and cell-based therapies, and interferon-based therapies are all being investigated (Skariyachan *et al.* 2020, Wang *et al.* 2020). Several already tested drugs/drug combos like antiviral, antiprotozoal drugs, immunosuppressive drugs, Chinese medicines, 3CLpro inhibitors, and jackfruit inhibitors are already being employed on a sizable amount of COVID-settled patients. Among them, some of the previously used medicines that have been repurposed are:

- Favipiravir (F),
- Ribavirin,
- Ivermectin,
- Vibramycin,
- Nitazoxanide/Azithromycin,
- Remdesivir,
- Oseltamivir, anti inflammatory,
- Lopinavir/ritonavir,
- Boceprevir,

- Telaprevir etc. (Kelleni 2020, Rana and Chowdhury 2020, Furuta *et al.* 2017, Chowdhury 2020, Zhang and Mylonakis 2021, Uzunova *et al.* 2020, Kumar *et al.* 2020, Padhi and Tripathi 2021) tool for scientists working on drug development (Padhi and Tripathi 2021).

Many anti-viral drugs are used in the treatment of the COVID-19 epidemic. In this thesis, the active ingredients favipiravir and ribavirin compounds, which are commonly used in treatment, will be studied. These drugs are known to inhibit various RNA and DNA viruses (Hagar *et al.* 2020).

Thermodynamic properties from the physical properties of favipiravir and ribavirin compounds will be investigated using Computational Chemistry Methods. In addition, it is aimed to investigate whether favipiravir and ribavirin compounds interact with DNA bases like adenine, guanine, cytosine, and thymine, or with which of them they interact more, using computational chemistry methods. It is planned to elucidate the structural properties of favipiravir and ribavirin compounds and DNA bases. These compounds and DNA bases have been calculated and interaction regions with DNA bases have been investigated.

1.1 Favipiravir

Favipiravir, also named T-705, was discovered when scientists were developing a treatment against the influenza virus by phenotypic assay. It was manufactured in Japan. Favipiravir includes a pyrazine analog that has undergone a chemical change (Figure 1.1). Evidence from clinical, laboratory, and animal studies has also indicated that favipiravir is a broad-spectrum drug against RNA viruses (Delang *et al.* 2018). Strict conditions have also been placed for the sale and manufacture of favipiravir under clinical use, due to the risks of teratogenicity and fetal toxicity (Nagata *et al.* 2015). Other drugs that have a broad-spectrum antiviral activity are ribavirin and interferon, but their destructive or harmful effects reduce their use in clinics. In human cells, when favipiravir enters the infected cells, an active structure called (favipiravir-RTP) or favipiravir ribofuranosyl-5′-

triphosphate, is formed by exposing favipiravir to further phosphorylation and phosphoribosyl (Figure 1.1) (Hashemian *et al.* 2021).

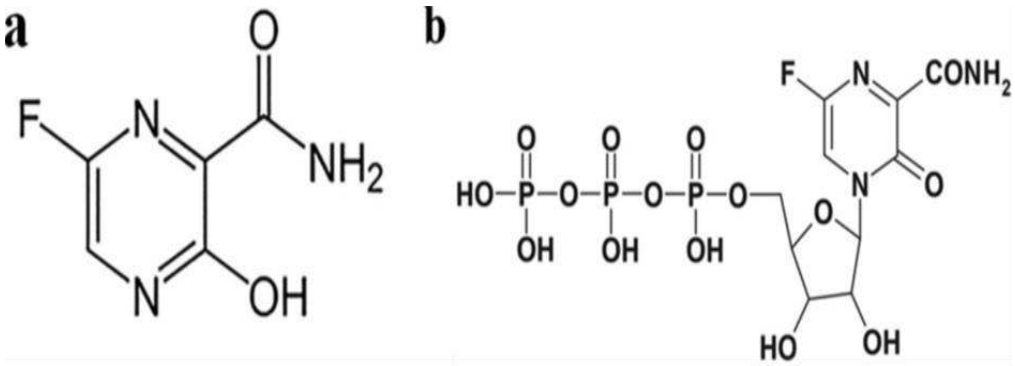

Figure 1.1 Chemical structures of (a) favipiravir (b) favipiravir-RTP represents the active structure of favipiravir (Hashemian *et al.* 2020)

However, the way that favipiravir-RTP works antiviral are unknown as of yet, but three hypotheses can be worked out: **a)** inhibition of the enzyme activity by a link of favipiravir-RTP together with the effective site of RdRp (Furuta *et al.* 2017) **b)** inhibition of additional RNA extension and inclusion missense in viral RNA for one or two sequences of favipiravir-RTP (Crotty *et al.* 2002, Streeter *et al.* 1973) **c)** lethal mutations (Figure 1.2) (Arias *et al.* 2014, Bassi *et al.* 2018) (Figure 1.2).

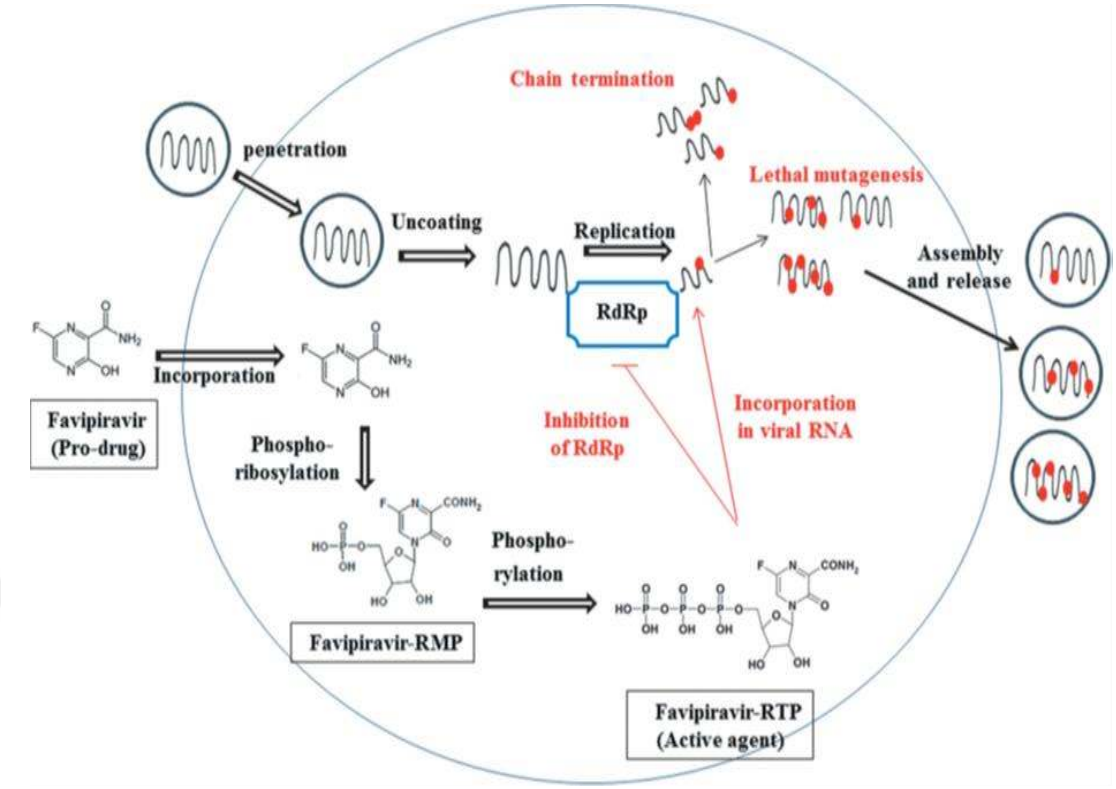

Figure 1.2 Favipiravir works in different ways, favipiravir can be incorporated intracellularly into favipiravir-RMP before favipiravir-RTP is formed, and RNA synthesis can be terminated by favipiravir incorporation into homologous viral RNA, or lethal mutations are formed by mysterious base conjugation in budding viral RNA, favipiravir-RTP indicated in the red spots could as well link to and inhibit RdRb (Hashemian *et al.* 2020)

1.2 Ribavirin

Ribavirin is a broad-spectrum antiviral drug and a good inhibitor of a group of RNA viruses and DNA viruses, Synthesized in 1972, the chemical structure of ribavirin consists of (1-B-D-ribofuranosyl-1, 2, 4-triazole- 3-carboxamide) as in Figure 1.3. Ribavirin was shown to be a good inhibitor of viruses that infect plants and animals, including tissue culture and animal models, as well as its effect on RNA and DNA viruses, including influenza, parainfluenza, herpes simplex viruses, and vaccinia (Snell 2001). Subsequent clinical trials were successful in treating RSV, hepatitis viruses, Lassa fever, measles, Hantavirus, and HIV infection (Fernandez *et al.* 1986).

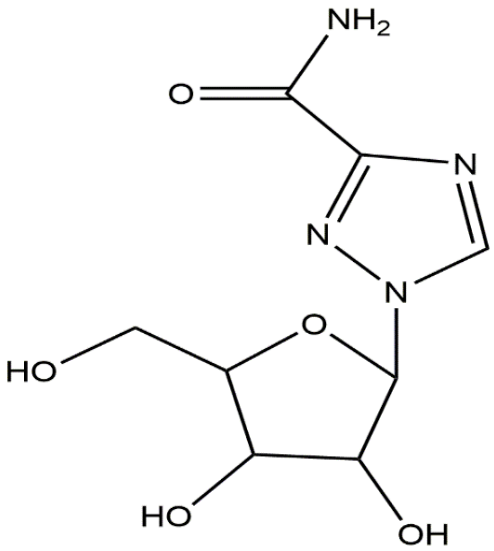

Figure 1.3 Chemical structure of ribavirin (Parniak *et al.* 2006)

2. LITERATURE REVIEW

DNA, short for deoxyribonucleic acid, is the genetic material found in all living things, most of the DNA is found in the cell nucleus, and the rest is found in mitochondria, structures inside the cell called (mtDNA) that get their energy from food and convert it into energy for us to use, cells work to store all the information of an organism and transmit it from one generation to another, as it carries the DNA of every protein produced in the body, it is known as the genetic code, and it includes all of the information required for an organism's development and growth, ensuring that every living organism has DNA of its own (Beck and Nielsen 2022). Nucleic acids were first observed by the scientist Friedrich Miescher in 1869 when he was developing methods for isolating the entire nucleus from the cell and chemically analyzing its contents, and that was in 1944. The basic structure of DNA consists of nucleotides that represent the basic molecules of DNA. Three elements make up a nucleotide: a sugar molecule, a nitrogen base, and a phosphate group. This phosphate group consists of a phosphorous atom attached to four oxygen atoms. The nitrogen group consists of four groups Adenine (A), Guanine (G), Thymine (T), Cytosine (C), and Uracil (U), and these letters work together to form the DNA genetic code (Blasie and Berg 2002). Nucleotides are linked to each other and form what is known as the double helix resulting from the structure of the two long strands that rise upwards as in Figure 2.1. The double helix structure is formed in the form of phosphate and sugar molecules at the edges of the ladder. The base pairs are rungs. Guanine alone with cytosine (G-C) (Blasie and Berg 2002). The arrangement of nitrogenous bases in DNA sequences produces genes that teach cells in the cell language how to make proteins, similar to the way letters in the alphabet can be organized to form words, genes encoding proteins as a shortcut for this process (Blasie and Berg 2002). However, DNA does not serve as a direct model for protein synthesis, or protein production.

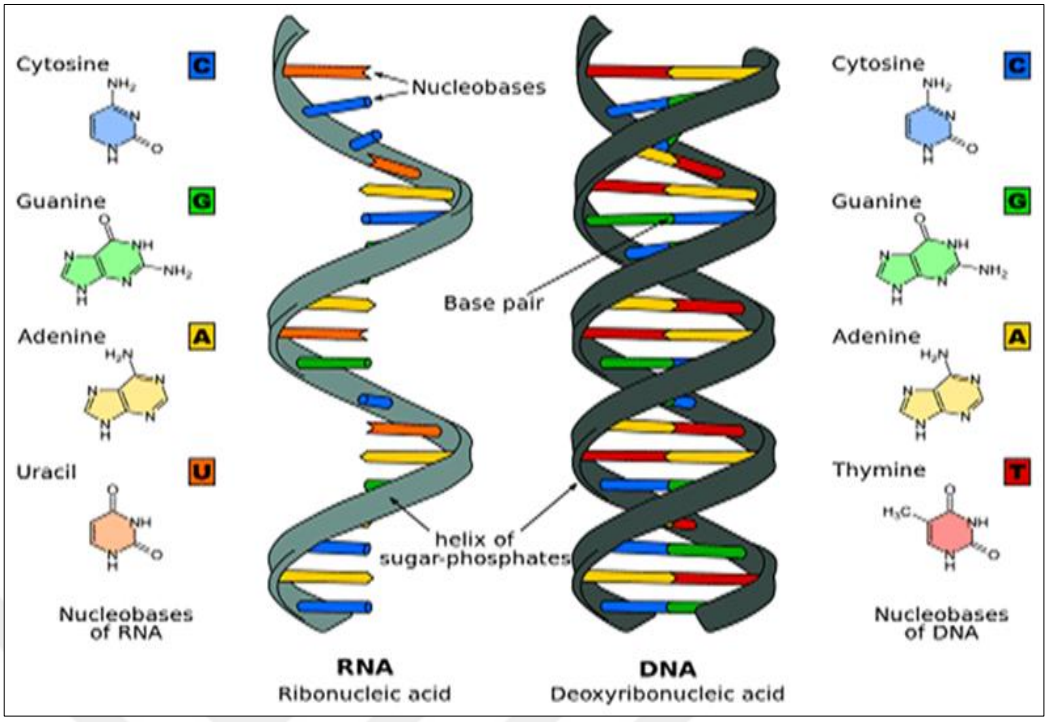

Figure 2.1 Nitrogenous bases (Helmenstine 2021)

2.1 Nitrogenous Bases

Nitrogenous bases are defined as organic chemicals with a similar periodic structure, which contains nitrogen, and they have an important role in biology (Hartwell *et al.* 2011). The nitrogenous base and as well as its structure stand in for the fundamental components of information interfaces that transport DNA and RNA molecules and play various biological functions the DNA molecule's backbone is found to be a nitrogenous base with a carbon sugar molecule and any of these bases are also referred to as nucleotides, Purines, and pyrimidines are the two primary groups of nitrogenous bases, each base in DNA and RNA has one thing in common: it is a ring-shaped hexagonal structure made up of 4 carbon atoms and 2 nitrogen atoms, while the purines base has an additional base with five sides made up of an extra carbon atom and two nitrogen atoms, the pyrimidine base only has one hexagonal ring (Hartwell *et al.* 2011, Krieger *et al.* 2004). The bonds within the single base are unique and work uniquely within the DNA, we find in DNA that there is a slight difference between them, this indicates that the nitrogenous base is present and the sugar ring has five carbon atoms, where we find four types of nitrogenous bases in DNA, namely adenine (A), thymine (T), cytosine (C), and guanine (G), while in RNA,

thymine is substituted by uracil (U) as a result of the structural resemblance between them, the dual rings consisting of nine members are referred to from adenine and guanine as purines, and six-member single-ring thymine, uracil, and cytosine are pyrimidines (Nelson and Cox 2008, Shen 2019). There are four types of nitrogenous bases in DNA (Figure 2.2).

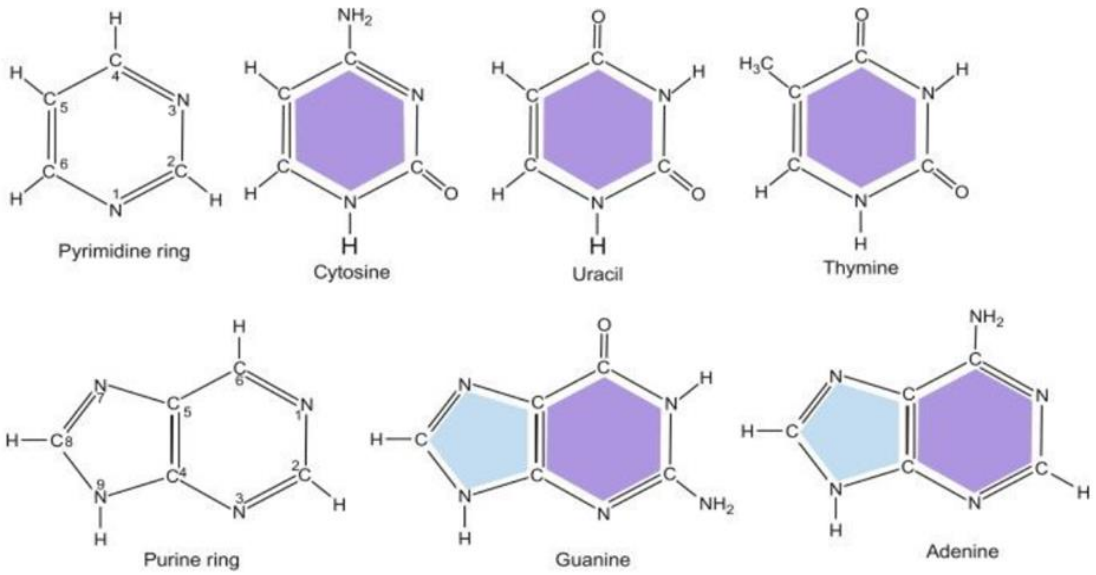

Figure 2.2 Chemical structure of the nitrogenous bases adenine, guanine, thymine, cytosine, uracil, pyrimidine, and purine in DNA and RNA (Shen 2019)

2.1.1 Adenine

Adenine is a nitrogenous base derived from the purine ring attached to the C6 position, which has an amino group inside. Adenine is usually denoted by the letter (A), and its auxiliary foundation in DNA is thymine, and adenine constitutes bonds with uracil in RNA, and adenine is denoted by the chemical formula $C_5H_5N_5$ as in Figure 2.2, adenine and other bases are attached either to phosphate groups or to a sugar Ribose or deoxyribose (2′-deoxyribose) to form nucleotides.

2.1.2 Guanine

Guanine is also called a purine and is referred to by symbol (G), the closed formula for guanine is $C_5H_5N_5O$ as in Figure 2.2, guanine binds with cytosine in both RNA and DNA, It is formed from the guanine nucleotide called guanosine, meat items include a lot of the diet's purines, specifically in the organs inside (such as the brain, liver, and kidneys), plants contain lesser levels of purines (such as beans, peas, and lentils).

2.1.3 Thymine

Thymine is also referred to as 5-methyluracil, and the token to thymine is the (T), and the closed formula for thymine is $C_5H_6N_2O_2$ as in Figure 2.2, thymine is a pyrimidine existing in DNA, thymine is bonded to adenine, and the corresponding nucleotide of thymine is thymidine (Nelson and Cox 2008).

2.1.4 Cytosine

Cytosine is indicated by the symbol (C), and the closed formula for cytosine is $C_4H_5N_3O$ as shown in Figure 2.2, cytosine binds with guanine in RNA and DNA, in the Watson-Crick model, DNA is created when cytosine and guanine make three hydrogen bonds, the nucleotide formed from cytosine is cytidine.

2.1.5 Uracil

The chemical element uracil is indicated by the symbol (U) and has the chemical formula $C_4H_4N_2O_2$, which can be considered demethylated thymine. In RNA, uracil binds to adenine to generate uridine nucleotides, as shown in Figure 2.2 (Hartwell *et al.* 2011).

Many additional nitrogenous bases can be found in nature, such as pyrimidine rings, which can be seen in nucleotides, thiamine (vitamin B1) and barbiturates. Other purines can be seen in nature, such as theobromine, xanthine, and caffeine (Nuevo *et al.* 2009).

3. MATERIALS AND METHODS

The materials and methods to be included in the thesis for different structures were studied before. Theoretical methods were used to elucidate the structures of favipiravir and ribavirin compounds. Gaussian 09 program (Iyengar and Frisch 2004) was used in the calculations. The basic program to be used in theoretical calculations is Gaussian 09, by selecting base functions such as B3LYP (Raghavachari 2000, Lee *et al.* 1988). In the calculations, basis sets like 6-311G(d, p) and 6-311+G(d, p) are selected. The geometric optimization, total energy, dipole moment, orbital energies of molecules, and thermodynamic properties of the favipiravir and ribavirin molecular structures will be computed for both gas and water media in their ground states. Comparison of electronic and structural parameters with literature data is among the main topics that physicists and chemists have worked on in recent years. The calculated bond parameters of the favipiravir and ribavirin molecular structures were compared with their experimental bond values in the literature.

3.1 Computational Chemistry

A collection of methods for using computers to investigate chemical issues is known as computational chemistry, often known as molecular modeling, the following issues are frequently looked into computationally: Molecule forms, including bond lengths, angles, and dihedral, are known as molecular geometry, molecule, and transition state energies provide information on which isomer is preferred at equilibrium as well as how quickly a reaction should proceed (based on the reactant and transition state energy) chemical reactivity, for instance, allows us to foretell the locations where different chemicals will attack a molecule by determining where electrons are gathered in large numbers (nucleophilic areas) and where electrons want to move (electrophilic areas), these spectra NMR, UV, and IR Could compute (Lewars 2011). Likewise, the way the enzyme and substrate interact: One strategy to produce better drugs is to look at how a chemical is compatible with the enzyme's active site. The material's physical characteristics are affected by the properties of individual molecules as well as by the interactions between molecules within the bulk substances. For instance, a polymer's force and fusion point are

determined based snugly for the molecules to coexist in harmony strength of the forces holding them together (Lewars 2011). A variety of techniques are available to computational chemists. The basic tools available fall into five basic categories: The molecular mechanic is built on the principle that molecules are made up of several atoms in the shape of balls kept by each other using bonds or springs from a specific set of pellets and springs, we could determine their energy if we are aware of plain spring dimensions and their angles as well as the amount of energy required to extend and bend the springs. To do a geometric optimization and determine the molecule's shape, the Engineering is adjusted till the lowest energy is accessed (Lewars 2011). A decent home computer can quickly optimize a reasonably large steroid molecule, such as a cholesterol compound ($C_{27}H_{46}O$), thanks to the speed of molecular mechanics. The Schrödinger equation serves as the basis for ab initio computations, which lean on basic principles. It is from of the basic equations of contemporary physics, it explains among others how electrons behave within a molecule. The Schrödinger equation for the molecule is solved using the ab initio approach which yields energy and a wave function. The distribution of electrons can be determined mathematically using the wave function. We can assess a molecule's polarity and which regions of it are more likely to be attacked by an electrophile or nucleophile by looking at its electron distribution (Lewars 2011). For each molecule containing more than one electron, it is impossible to accurately calculate the Schrödinger equation, so the principle of approximations is used and the less important the greater, the degree of ab initio computation. No matter how complex it is, a novice computation is the "first principle" in the sense that it is simply based on the fundamental physical theory (quantum mechanics). The IR spectra and geometry, of propane, could be computed at a reasonable grade on a desktop computer in a few minutes however in a massive molecule such as a steroid it takes several days, ab-initio computation is rather slow, the most recent personal computers may vie at present with UNIX workstations for challenging tasks related to higher performance ab-initio computations since they have 2 GB or more RAM and 1,000 GB or more of available disk space (Lewars 2011). The Schrödinger equation is the basis for semi-empirical computations (ab initio) as it is solved, more approximations are made on it, and the program derives from a collection of integrals that was created by selecting the solutions that fit certain computed entities such as geometry or energy (heat of formation) to the empirical values Rather than the

actual evaluation in quasi-empirical computations, of the extremely complicated For integrations that must be computed using the ab initio approach. Mathematical equations for integrating experimental values to obtain the most accurate calculated results are referred to as (parameters) (Lewars 2011). Ab initio calculations are substantially quicker than semiempirical computations, which are slower than molecular mechanics. Molecular mechanics calculations take around 100 times longer than semiempirical calculations, in contrast, ab-initio computations average 100–1.000 twice as times as semi-experimental computations. An improvement of a steroid's semiempirical topology just may require a few seconds on a computer. The Schrödinger equation serves as the foundation for density functional calculations (also known as DFT computations or density functional theory), ab-initio calculations, as well as semi-experimental computations. The electron distribution (electron density function) is directly derived using DFT, in contrast to the other two techniques, which compute a conventional wavefunction (Lewars 2011). Calculations based on density functional theory are often later than semiempirical however quicker than ab-initio. DFT is not that old, the ab initio with semiempirical computational chemistry was conducted in the 1960s and significant DFT computational chemistry began in the 1980s. Calculations of molecular dynamics treat molecules as moving objects. Therefore, one may create a model of an enzyme's movement as it transforms into a reactant or the movement of a bevy of water molecules as they encircle a molecule of liquid. Atomic and molecular dynamics in quantum mechanics enable the simulation of genuine chemical processes (Lewars 2011). Computational chemistry is helpful in materials science or the study of the characteristics of materials. Computational chemistry has been used to study every one of these elements, including porcelain, polymers, superconductivity, and semiconductor. These topics are usually somewhat specialized and require a working understanding of solid-state physics. Compared to experiments, computational chemistry is faster, cheaper, and safer for the environment Despite the abundance of computers during the past ten years has increased concerns about energy consumption and the disposal of old machines after them. And computational chemistry does not take the role of an experiment, which is still the ultimate arbiter of what is real nature (Lewars 2011).

3.2 Density Functional Theory (DFT)

In this thesis, we will rely on the density functional theory (DFT), to calculate the molecule favipiravir (T-705) and ribavirin, the (DFT) is an electronic structure style used to predict molecular, crystalline, and atomic characteristics, where the objective is to fully extract information contained in density (as opposed to the wave function) of the system in ground state unborn. Because DFT requires less computing power than dual group (CC) approaches, it is one of the most widely utilized tools in theoretical chemistry, for example, for systems with a hundred or more atoms. It wasn't always like this. DFT was mostly relevant to solid states before the middle of the 1980s, where straightforward methods based on the unified electron gas model frequently perform well. Complex estimates were needed for difficulties in chemistry (Dykstra *et al.* 2005). An express mathematical equation is known as functional energy density that will determine the relationship between system density and ground state energy is still elusive (Cohen *et al.* 2012). Although the Hohenberg-Kohn theory proves that this function exists and is accessible through reducing functional density (Cramer 2013). The principal difficulty facing the DFT even today lies in determining the functional approximation of "unknown" energy density. Moreover, users of computational chemistry packages must be aware of the benefits and drawbacks of the functions they choose since the effectiveness of DFT approaches heavily depends on the function selection within a specific chemical problem, and thus it is not surprising that many studies are devoted to rating the performance of DFT functions (Tyminska 2013).

In addition to the previously described pure DFT functionals, another variety, known as hybrid functionals is also often utilized, constructed by hybridization the E_X^{HF}, that is determined by the HF-exchange equation, with E_X and E_C GGA or mGGA terms. For an illustration of hybrid GGA, we'll go into greater depth on the B3LYP function. Becke's three-parameter function is the B3LYP variant that is implemented in Gaussian (Becke 1993). In this case, the association functional is PW91 (Perdew *et al.* 1992, Perdew *et al.* 1993). Is replaced with the functional link by Lee-Yang-Parr (LYP) (Lee *et al.* 1988). Consequently, the unadjusted B3LYP method is provided by Equation (3.1).

$$E_{XC}^{B3LYP} = a_0 E_X^{HF} + (1 - a_0) E_X^{LDSA} + a_X \Delta E_X^{B88} + E_C^{LSDA(PW92)} + a_C \Delta E_C^{LYP} \quad (3.1)$$

where Equation (3.2);

$$a_0 = 0.20, a_X = 0.72, a_C = 0.81 \quad (3.2)$$

The values of these empirical parameters (a_0, a_X, a_C) were improved for B3PW91 by fitting a sequence of ionization potentials, atomic energies, proton affinities, and atomization energies of systems constructed from elements in the initial 2 lines of the periodic table (Raghavachari 2000). The E_X^{HF} is the Hartree-Fock exchange energy, E_X^{LSDA} is Slater's LSDA method, ΔE_X^{B88} is the GGA B88 exchange (Becke and Roussel 1989), $E_C^{LSDA(PW92)}$ is Perdew-Wang parameterizations (Perdew and Wang 1992) of LSDA correlation, and ΔE_C^{LYP} is GGA LYP correlation.

The expression in Equation (3.1) LYP cannot be split into local and non-local link expressions, hence the model must be adjusted (Stephens *et al.* 1994), therefore instead of $E_C^{LSDA(PW92)}$ the (1−ac) E_C^{VWN} term is employed, resulting in the B3LYP formula as Equation (3.3)

$$E_{XC}^{B3LYP} = 0.2 E_X^{HF} + 0.8 E_X^{LSDA} + 0.72 \Delta E_X^{B88} + 0.19 E_C^{VWN} + 0.81 \Delta E_C^{LYP} \quad (3.3)$$

The above equation specifies the original expression for B3LYP, this differs from the Gaussian software package's default B3LYP (Dykstra *et al.* 2005), so we only note here that the VWN (Vosko *et al.* 1980) a crucial element that varies between B3LYP variations is the term. More specifically, the default B3LYP function in the Gaussian scenario has the equation shown in Equation (3.4):

$$E_{XC}^{B3LYP} = 0.2 E_X^{HF} + 0.8 E_X^{LSDA} + 0.72 \Delta E_X^{B88} + 0.19 E_C^{VWN1-RPA} + 0.81 \Delta E_C^{LYP} \quad (3.4)$$

where, as an improvement over the not local treatment of electron-electron interconnection, RPA stands for the Random-Phase Approaches to the density functional connexion energy, an illustration of a hybrid (mGGA) functional is TPSSh (Tao *et al.* 2003).

In short, there are many estimates of the accuracy of the DFT so that the exchange correlations can be arranged according to the following method (Grimme *et al.* 2012).

- LDA where the electron density alone determines the exchange-connexion functional
- When both ρ and ∇ρ are present, GGA is used
- mGGA that includes ρ and ∇ρ and in addition to $\nabla^2\rho \; or \; \tau$
- Hybrid functionalities that combine accurate (HF) exchange
- hybrid functionals with two levels that increase accreditation on hypothetical (KS) orbitals

3.2.1 Time-dependent DFT

Electronic excitations, which are time-dependent processes for characterizing photon-electron reactions, may be used to model the excited state of molecules or atomic systems using Time-Dependent (TD) DFT, a time-dependent version of the Hohenberg-Kohn theorem is the Runge-Gross (RG) theorem; for the primary non-deteriorate state Ψ_0 and the temporal development of electron density, it ensures the presence of a specifically determined external potential ρ (r, t), the RG theorem determines seeming action integral (A), described by Equation (3.5), it is viewed as a density functional:

$$A[\rho] = \int_{t0}^{t1} dt \, \langle \Psi[\rho](r,t) \, \big| \, i \, \frac{\partial}{\partial t} - \hat{H}(r,t) \, \big| \, \Psi[\rho](r,t) \, \rangle \qquad (3.5)$$

This is important since the total energy of time-dependent systems is not preserved and the difference precept cannot be simply applied to discover the energy, however, the difference of A [ρ] to ρ(r, t) may be discovered, and the time-dependent KS equations can be solved to get the system's precise density.

3.3 Schrödinger's Equation

The Schrödinger equation is the basis of theoretical chemistry, it is given as follows Equation (3.6).

$$\widehat{H}\Psi = E\Psi \tag{3.6}$$

where E is the system's energy, Ψ is the wavefunction (the eigenfunction for a particular Hamiltonian), and $\widehat{H}$ is the Hamiltonian operator. The following Equation (3.7) results from the wavefunction's description of the system, which uses the positions of the system's electrons and nuclei as variables.

$$\widehat{H}\Psi_i(\vec{x}_1, \dots, \vec{x}_N, \vec{R}_1, \dots, \vec{R}_M) = E\Psi_i(\vec{x}_1, \dots, \vec{x}_N, \dots, \vec{R}_1, \dots, \vec{R}_M) \tag{3.7}$$

When Ψ is known, the properties of the system can be inferred from $\vec{x}_N$, which describes the electrons' locations, N and $\vec{R}_M$, which describes the locations of the atoms' nuclei (Davin 2009).

3.4 The Born-Oppenheimer Approximation

As we saw earlier, the positions of the system's nuclei and electrons both affect how the wave functions (Ψ) behave. The nucleus' movements relative to electrons are minimal, though, because it is around 1900 times heavier than the electron. It can be said to be frozen in this situation, with its kinetic energy Adjusted to zero, but it nevertheless adds to the system's potential energy. Meanwhile Ψ it depends solely based on the electrons' kinetic energy (T_e), nuclear electron gravity (V_{ne}), and the opposition between electrons (V_{ee}) hence, the Hamiltonian changes as in Equation (3.8) (Rybkin 2014).

$$\widehat{H} = -\frac{1}{2}\sum_{i=1}^{N}\nabla_i^2 - \sum_{i=1}^{N}\sum_{A=1}^{M}\frac{Z_A}{r_{iA}} + \sum_{i=1}^{N}\sum_{j>i}^{N}\frac{1}{r_{ij}} + V_{nn} \tag{3.8}$$

As that V_{nn} is constant and it indicates opposition between nuclei, we note that Equation (3.8) is factorizable. In this case Equation (3.9);

$$\widehat{H}_{elec} = \sum_i \left(-\frac{1}{2}\nabla_i^2 - \sum_A \frac{Z_A}{r_{iA}} + \sum_{j>i} \frac{1}{r_{ij}} \right) \tag{3.9}$$

3.5 The Slater Determinant

The wave function endogeneity mechanism (Ψ) is not visible on its own but through the following Equation (3.10) it is possible,

$$|\Psi(\vec{x}_1, \vec{x}_2, \dots, \vec{x}_N)|^2 \, d\vec{x}_1 d\vec{x}_2 \dots . d\vec{x}_N \tag{3.10}$$

where $(d\vec{x}_1 d\vec{x}_2)$ a small volume representing the probability of finding an electron in a certain location in space, since the electrons are indistinguishable, the exchange of two electrons does not change the probability as in Equation (3.11);

$$\left|\Psi(\vec{x}_1, \vec{x}_2, \dots, \vec{x}_i, \vec{x}_j, \dots, \vec{x}_N)\right|^2 = \left|\Psi(\vec{x}_1, \vec{x}_2, \dots, \vec{x}_j, \vec{x}_i, \dots, \vec{x}_N)\right|^2 \tag{3.11}$$

However, the exchange of two electrons changes the indication of the wavefunction, i.e. Ψ is asymmetric about the alteration of the electron, Since two electrons could not be existing in the same condition, this interprets the Pauli exemption precept in a quantum mechanical way.

Since the precise wavefunction is uncertain, it is essential to construct an empirical wavefunction subject to this asymmetry principle, to do this the N-electron wavefunction is expressed as the asymmetric product of the N-wave functions for a single electron $x_i(\vec{x}_i)$, this item is marked Φ_{SD} and is known as Slater specific as in Equation (3.12);

$$\Phi_{SD} = \frac{1}{\sqrt{N!}} \begin{vmatrix} x_1(\vec{x}_1) & x_2(\vec{x}_1) & \cdots & x_N(\vec{x}_1) \\ x_1(\vec{x}_2) & x_2(\vec{x}_2) & \cdots & x_N(\vec{x}_2) \\ \vdots & \vdots & \ddots & \vdots \\ x_1(\vec{x}_N) & x_2(\vec{x}_N) & \cdots & x_N(\vec{x}_N) \end{vmatrix} \quad (3.12)$$

The rows correspond to the electron indicators, while the columns correspond solo electron wavefunctions (orbits), denoted by $x(\vec{x})$ (Szabo and Ostlund 2012).

3.6 Hartree-Fock Theory (HF)

The Hamiltonian may be split into two sections in the Hartree-Fock technique of the nuclei Hamiltonian H_i^c, which interpret the kinetic energy and Earning possibilities of (electron cores), with the portion that exemplifies disharmony (Both electrons), As in the following Equation (3.13)

$$H = \sum_i \left[H^c(i) + \sum_{j>i} \frac{1}{r_{ij}} \right] with\ H^c\ (i) = -\frac{1}{2}\nabla_i^2 - \sum_A \frac{Z_A}{r_{iA}} \quad (3.13)$$

The (electron and electron) dissonance component can only be handled in an intermediate manner, where each electron is thought to be traveling independently of the others in an intermediate field formed by the other electrons, where can Hamiltonian essence can be rectified entirely.

By using a lone Slater variable to calculate the variance, Φ_{SD}, by maximizing the x_i orbitals, the minimal energy may be calculated. The optimal rotation orbits in whose E achieves its minimal value are identified by the solving of the resulting equations, which are known as Hartree-Fock as in Equation (3.14);

$$\hat{f}_i x_i = \epsilon_i x_i \quad (3.14)$$

(x_i) is an inherent function for the ($\hat{f}$) laborer, commonly which is referred to as the Fock laborer, and (ϵ_i) is the associated energy, which denotes the orbital energy, the eigenvalue

of a Fock laborer linked to orbital rotation negative value $(-\epsilon_i)$, depending on Koopmans, this value coincides with the ionization possibility. The single-electron Fock laborer is an efficient laborer of the form and it is expressed in (Figure 3.1)

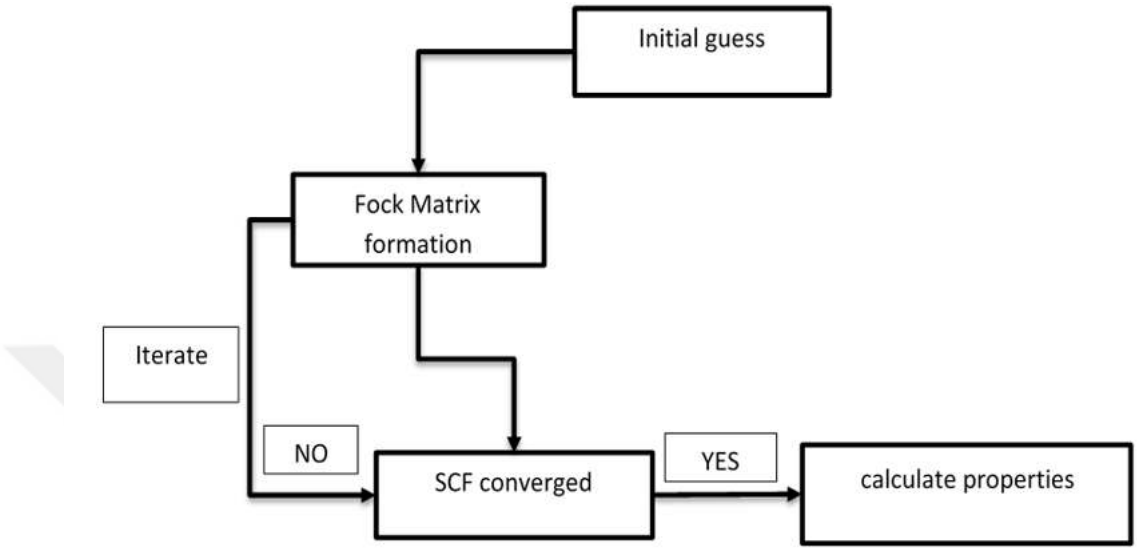

Figure 3.1 The Hartree-Fock approach to SCF cycle use (Davin 2009)

3.7 Electron Correlation

The primary issue with the higher frequency method's solutions is that the total power gained is consistently higher than the actual power, this is mostly because the electrons are assumed to flow in a medium electronic field in the Hartree-Fock approach, Therefore, the velocity of each electron about the others is not included. The connexion energy is used to define the distinction between the actual and HF energies as in Equation (3.15);

$$E_{correlation} = E_{total} - E_{HF} \tag{3.15}$$

Electronic bound energy is represented by this hole, which in most circumstances correlates associated, is around (1%) of overall energy, however, this (1%) has the potential to significantly affect the system's computed attributes, the customary method for introducing correlation is to consider the excitement with a single or so more electron

from filled orbitals to default orbitals with maximal energies. It is represented in Figure 3.2 (Davin 2009).

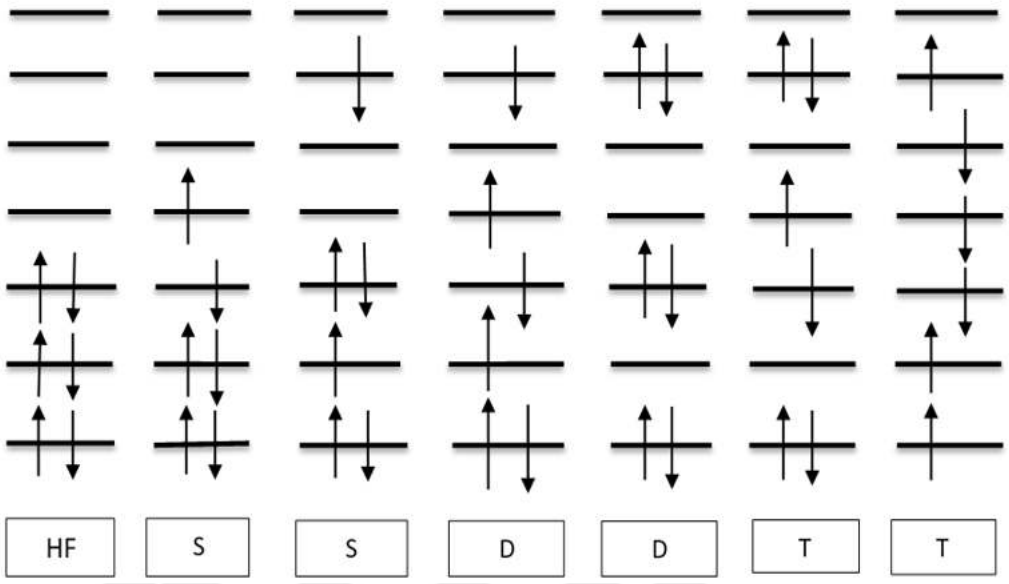

Figure 3.2 Potential electrons redistribution for single, double, and triple hypothetical excitement (Davin 2009)

A Slater specific is used to characterize every state, and the summation of these determinants results in a new trial function that should be more accurate than the authentic determinant in representing the veritable system.

3.8 Basis Sets

Base functions are frequently widened as a lineal group of these functions with a defined set of transactions, are employed to create atomic orbits (AO) or molecular orbits. There are two categories into which these fundamental functions can be divided.

Slater-model orbits, commonly known as STO_S, exhibit exponential reliance: $e^{-\varsigma r}$, and are extremely near to the real number in their mathematical characterization (AO) the Gaussian-model orbits, commonly known as GTO_S, have exponential reliance $e^{-\alpha r^2}$.

Utilizing polarization functions (and/or) diffuse functions, basis groups can be expanded. Atomic bonds cause the electronic cloud surrounding every atom to deform, a process known as polarization. Functions with top angular momentum are genitive to the basis set to enable this. For instance, polarization is enabled by the addendum of a P to H function. Similarly to this, a d-function can be genitive to a basis set that Includes P-valence orbits, and addition f-functions for d-valence orbits. The included polarization functions can be more precisely specified for more accurate results: for instance, polarization functions (d, p) can be added to a hydrogen atom's 6-311G basis set, and the basis set changes to 6-311G(d, p). The diffusion functions are denoted by a plus sign (+), and when the polarization functions (d, p) are added to them, they become on this formula 6-311+G(d, p), concerning the region of atomic orbits that are located far from the nucleus and can have a significant role when discussing anions or prevalent electronic clouds in second- or third-lineup transmission minerals (Davin 2009).

3.9 HOMO and LUMO Analysis

The two primary orbitals that contribute to chemical stability are the lowest molecular orbital that is vacant (LUMO) and the highest molecular orbital that is busy (HOMO), the nature of reactivity and some of the structural and physical characteristics of molecules may be understood through the use of molecular orbitals (Gunasekaran *et al.* 2008). The HOMO stands for the capacity to provide an electron, whereas the LUMO stands for the capacity to receive an electron, when a single electron is excited from the highest occupied molecular orbital to the lowest empty molecular orbital it effectively describes electron transition absorption, which corresponds to the transition from the ground to the first excited state (Atalay *et al.* 2008, Kurt *et al.* 2011). The HOMO of nature is evenly distributed across the ring, LUMO of nature, in contrast, is delocalized throughout the full portion of the molecule. Therefore, an energy transfer from the aromatic heterocyclic ring is implied by the HOMO to LUMO transition, the energy gap gauges the molecules' kinetic stability, and a molecule becomes more polarizable when it has a tiny border orbital gap, which suggests high chemical reactivity and poor kinetic stability (Magdaline and Chithambarathanu 2015) (Figure 3.3).

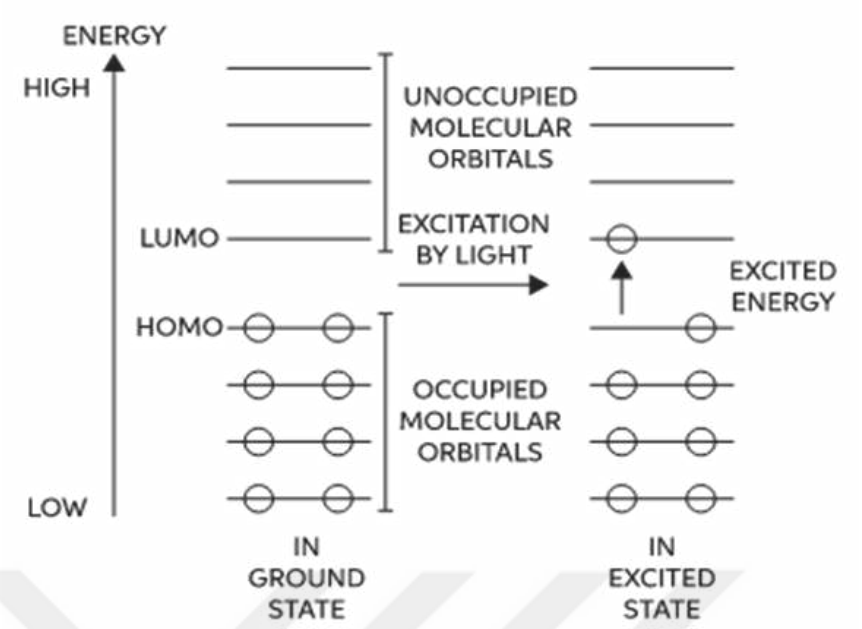

Figure 3.3 Illustration of the HOMO and LUMO molecular orbitals

3.10 Thermodynamic Properties

Thermodynamics is one of the branches of science that deals directly with heat, and it is composed of two words, the word thermo, which means (heat) and the word dynamics, which means (force), the first appearance of the principle of thermodynamics in the nineteenth century, previously, thermodynamics only dealt with a hot object represented by heat engines to make it more efficient, nowadays, thermodynamics has begun to deal with energy and its relationship to the properties of matter, the thermodynamic content is represented by the amount of matter present within its boundaries and everything that comes out of these boundaries is called the environment, most of the environment contains ideal heat reservoirs, as well as containing heat sources with infinite heat capacity, which makes it able to abandon heat absorption without a change in its temperature (Ghassemi and Shahidian 2017). Thermodynamic limits can be imaginary, real, moving, or stationary, in addition to the presence of two types of systems, the open system and the second closed system, in an open system, the volume can be controlled where the amount of mass is not fixed, and the mass can cross the boundaries of the system, that is, the open system has the ability to interchange energy and matter with its perimeter, in a closed system, the control mass is fixed, that is, the system contains a fixed

amount of matter, and this means that the mass cannot cross the boundaries of the system, that is, the closed system can only exchange energy with its perimeter (Ghassemi and Shahidian 2017). Thermodynamics is a macroscopic property of a living body, that is, a numerical value can be assigned to it at a specific time regardless of date, and this property is either wide-ranging or intense, if it is large-scale, it depends on the extent of the system or the size, such as mass and volume, as for condensation, it is found at some point in space, such as density, pressure, and temperature, there are intensive properties that are used to describe the behavior of materials, the three most important of which are specific volume, pressure, and temperature, the amount of cubic meters that one kilogram of any substance may occupy is the specific volume, pressure can be defined as the force exerted on a surface per unit area, the temperature is a measure of the temperature and coldness of an object and is sensed by a thermometer (Ghassemi and Shahidian 2017).

3.10.1 Entropy

Entropy is a measure used to determine the random ratio and turbulence of a thermodynamic system, which means that its value changes with the change in the amount of matter present. Entropy is measured in joules per kelvin (j/k). We also find that entropy has a property either negative or positive according to thermodynamics, entropy, according to the second law of thermodynamics represents thermal inertia, a measure used to measure the tendency of any closed system to spontaneous transformation using the goal of reaching a state called the state of equal distribution within all Parts, such as isothermal heat, equal pressure, or equal density. The principle of entropy means the process of dissipating the existing heat. The value of the entropy changes with the change in the amount of matter, which means that the greater the disorder of the substance in the medium and the greater the scattering of its particles in different directions, the greater the value of the entropy, while the value of the entropy decreases when the disorder of the substance decreases and the diffusion of its particles in the medium decreases and the system becomes ordered, Entropy is indicated by the symbol (S). An example of entropy is the transformation of water from the liquid state to the gaseous state, where the energy of the system increases with the increase in the rate of evaporation of water when it turns

from liquid to gas, and when the number of transformations increases, the chaos increases and thus the entropy increases.

3.10.2 Enthalpy

Enthalpy is a tool for measuring the energy of the thermal system within a thermodynamic group, and it is indicated by the symbol (H), and enthalpy is also referred to as the product of the internal energy and symbolized by it (E) with the product of pressure multiplied by the volume, where it symbolizes the pressure (P) and symbolizes The volume (V) is denoted by the Equation (3.16).

$$H = E + PV \tag{3.16}$$

Since it is difficult to determine the zero point, the total enthalpy of the system cannot be measured, and therefore the change in enthalpy is measured instead of enthalpy, in addition to the possibility of determining the enthalpy difference between different states, and under the influence of constant pressure the enthalpy change can be measured, as in Equation (3.17).

$$\Delta H = E + P\Delta V \tag{3.17}$$

The enthalpy is crucial in determining whether a reaction is exothermic or one that undergoes a negative change in enthalpy, an endothermic reaction, or one that undergoes a positive change in enthalpy, the enthalpy change is used to measure heat flow in calorimetry and to calculate the heat of a chemical reaction, Enthalpy measurements are used to determine the minimum power required for the compressor and to assess the Thomson-Joule expansion or throttling process.

3.10.3 Heat capacity

The heat capacity of a substance is the amount of heat necessary to increase its temperature by one unit while preventing phase transitions in a given mass of the substance, sometimes referred to as thermal capacity, the ability of a material to soak up heat energy is described, the sample's size and mass have an impact on heat capacity which is a broad attribute, the converse of this is that if the sample contains twice the quantity of the other sample material, therefore to achieve the same change in temperature, two times as much heat energy (Q) is required. The heat capacity equation is written according to Equation (3.18).

$$C = \frac{\Delta Q}{\Delta T} \tag{3.18}$$

In the SI, where C represents the amount of heat capacity measured in units (J/K), ΔQ represents the change in the amount of heat measured in joules (J), and ΔT represents the change in temperature and its unit Kelvin (K).

Heat capacity at constant pressure and volume is written as C_p and C_v respectively, regardless of sample quantity, derived heat capacity quantities are specified by molar heat capacity, which refers to a specific heat capacity and heat capacity per mole of pure material, often referred to as "specific heat" and still indicated by the letter C, which is heat capacity per unit mass from materials for example (kJ/kg C), they are derived quantities that define heat capacity as a condensing property, regardless of sample size, in certain cases, it is more practical to indicate the heat capacity of material using unit volume rather than unit mass (Sheng and Zeng 2022).

4. RESULTS AND DISCUSSION

Due to the COVID-19 virus's propensity for antigenic mutation and treatment resistance, the hunt for new antivirals is a major goal of medical science and healthcare systems. Several experimental medications have been tested against COVID-19 (Allam *et al.* 2020); favipiravir and ribavirin are the medications identified as being effective against DNA and RNA-viral contagions of COVID-19 (Furuta *et al.* 2009) as broad-spectrum inhibitors (Furuta *et al.* 2013). Experimental treatment with favipiravir for COVID-19 (Caly *et al.* 2020, Rhyman *et al.* 2018) has provided early data supporting the prevention of SARS-CoV-2 virus infection (Soliman and Aal 2021). Many properties of favipiravir and ribavirin drugs have been studied before. In this study, optimization, energy values, thermodynamic properties, and interaction with DNA bases were investigated by using computational chemistry methods in gas and solvent environments with different basis sets in order to shed light on other researchers.

Chemical diagrams of favipiravir and ribavirin (virazole) compound used in theoretical calculations are given in Figure 4.1 and Figure 4.2. The structural formula of the favipiravir compound is 6-fluoro-3-hydroxypyrazine-2-carboxamide. The structural formula of the ribavirin compound is 1-(3,4-dihydroxy-5-(hydroxymethyl) tetrahydrofuran-2-yl)-1*H*-1,2,4-triazole-3-carboxamide.

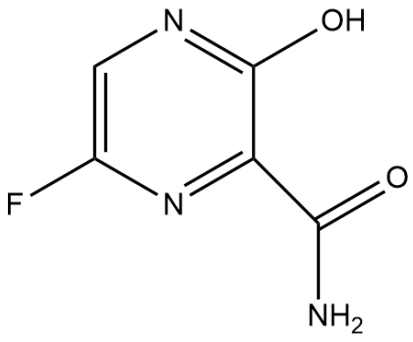

6-fluoro-3-hydroxypyrazine-2-carboxamide
(Favipiravir)

Figure 4.1 The chemical diagram of 6-fluoro-3-hydroxypyrazine-2-carboxamide (Favipiravir)

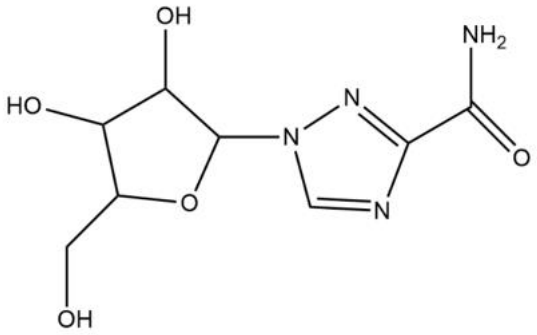

1-(3,4-dihydroxy-5-(hydroxymethyl)tetrahydrofuran-2-yl)-1*H*-1,2,4-triazole-3-carboxamide (Ribavirin)

Figure 4.2 The chemical diagram of 1-(3,4-dihydroxy-5-(hydroxymethyl) tetrahydrofuran-2-yl)-1H-1,2,4-triazole-3-carboxamide (Ribavirin)

The CIF files containing the atomic coordinates of the compounds favipiravir (CCDC number 969968) (Babashkina *et al.* 2022) and ribavirin (CCDC number 1284473) (Prusiner and Sundaralingam 1976) have been downloaded from the Cambridge Structural Database (Groom *et al.* 2016). One method used in computational chemistry is (DFT), and it may be used for: geometric optimization of the molecular structures of favipiravir and ribavirin compounds, frequency calculation, and energy calculation made in the ground state. The atomic coordinates of the compounds used in the calculations were taken from the literature (Babashkina *et al.* 2022, Prusiner and Sundaralingam 1976) to reduce the calculation time.

4.1 The Optimization Studies of the Favipiravir and Ribavirin Molecular Structures

Favipiravir compound with closed formula $C_5H_4FN_3O_2$ consists of a six-membered aromatic ring, pyrazine ring, and carboxamide group. Ribavirin compound with closed formula $C_8H_{10}N_4O_5$ consists of a five-membered furan and triazole rings and carboxamide group.

Geometric optimizations of the favipiravir and ribavirin molecular structures were performed in both gaseous and water environments with different dielectric constant and polarity at the ground state by the DFT/B3LYP method and the 6-311G(d, p) and 6-

311+G(d, p) basis sets. The dielectric constant and dipole moment of the water solvent is, μ=1.82 D, ε=80.1. Polarity is influenced by the dielectric constant, which increases (in this study; water=high, gas phase=low). Another effect is the dipole moment. The optimized molecular structures of the favipiravir and ribavirin are given in Figure 4.3 and Figure 4.4.

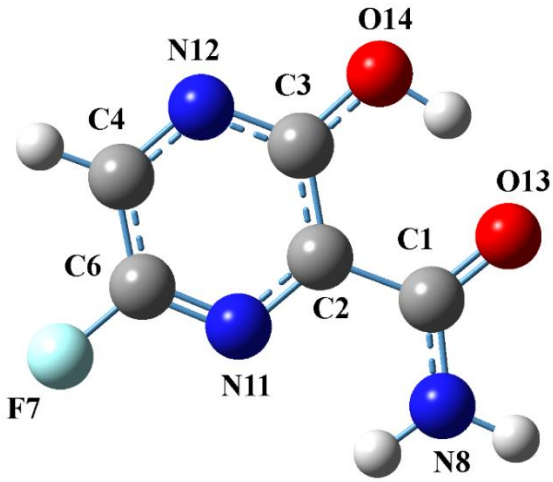

Figure 4.3 The optimized molecular structure of the favipiravir by DFT/B3LYP (6-311+G(d, p) in a water medium

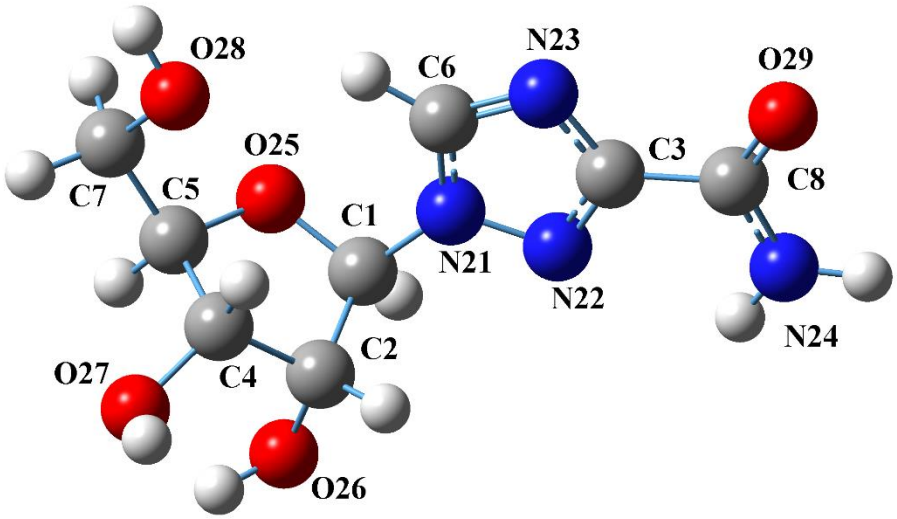

Figure 4.4 The optimized molecular structure of the ribavirin by DFT/B3LYP (6-311+G(d, p) in a water medium

The bond parameters of the optimized molecular structures of the favipiravir and ribavirin were compared with their experimental bond parameters in the literature and the bond parameters are given in Table 4.1. The best measure of how well experimental data fit a linear curve is regression. Regression analysis was performed to investigate the compatibility between the calculated bond parameters of the optimized molecular structures and their experimental parameters, and the results are given in Figure 4.5 and Figure 4.6. As can be seen from Figure 4.5 and Figure 4.6 with Table 4.2, it can be said that the bond lengths calculated for the favipiravir compound are better matched to the empirical values in the literature by the B3LYP/6-311+G(d, p) method and the water environment, and the bond angles in the same method and the gas environment. It can be said that the calculated bond lengths and bond angles for the ribavirin compound are more compatible with the experimental values in the B3LYP/6-311+G(d, p) method and in water media. Regression is the most accurate way to assess how well experimental data fit a linear curve. The findings of regression analysis, which was used to examine the compatibility between the optimized molecular structure's calculated bond parameters and its experimental parameters, are shown in Figure 4.7 and Figure 4.8.

Table 4.1 The calculated and experimental geometrical bond parameters of the favipiravir

Favipiravir	**Exp. (Babashkina *et al.* 2022)**	**B3LYP 6-311G(d, p) Gas**	**B3LYP 6-311G(d, p) Water**	**B3LYP 6-311+G(d, p) Gas**	**B3LYP 6-311+G(d, p) Water**
Bond lengths (Å)					
C1-N8	1.318(2)	1.34488	1.33656	1.34616	1.33671
C1-O13	1.244(2)	1.23651	1.24318	1.23704	1.24482
C1-C2	1.481(2)	1.49159	1.49324	1.49124	1.49297
C2-N11	1.335(2)	1.34031	1.33864	1.34039	1.33873
N11-C6	1.295(2)	1.30364	1.30361	1.30223	1.30173
C6-F7	1.339(3)	1.34143	1.34375	1.34412	1.34728
C6-C4	1.390(3)	1.39892	1.39688	1.39876	1.39679
C4-N12	1.306(3)	1.32288	1.32582	1.32292	1.32567
N12-C3	1.340(2)	1.33898	1.33707	1.33794	1.33600
C3-O14	1.328(2)	1.32591	1.33095	1.32703	1.33282
C3-C2	1.397(2)	1.41488	1.41324	1.41557	1.41338
R^2		0.97892	0.98685	0.97823	0.98726
Bond angles (°)					
O13-C1-N8	123.07(15)	123.58824	123.75419	123.44708	123.64297
C6-N11-C2	116.26(18)	117.06983	117.13939	117.13424	117.20695
O14-C3-N12	115.63(16)	116.90688	116.75080	116.81136	116.63109
O14-C3-C2	123.53(15)	122.66827	122.47117	122.70612	122.50744
N11-C6-F7	116.8(2)	117.77050	117.44691	117.62527	117.27211

Table 4.1 The calculated and experimental geometrical bond parameters of the favipiravir (Continued)

Favipiravir	Exp. (Babashkina *et al.* 2022)	B3LYP 6-311G(d, p) Gas	B3LYP 6-311G(d, p) Water	B3LYP 6-311+G(d, p) Gas	B3LYP 6-311+G(d, p) Water
F7-C6-C4	119.87(17)	119.47399	119.45078	119.40991	119.36664
R^2		0.96601	0.95719	0.97183	0.96081
Torsion angles (°)					
N8-C1-C2-C3	179.68(16)	-179.98418	179.98192	179.97614	179.98112
O13-C1-C2-N11	179.23(17)	179.97930	179.99065	179.98803	179.99160
O14-C3-N12-C4	-179.79(19)	-179.99761	179.98875	179.98679	179.98935
N11-C2-C1-N8	-0.4(2)	0.01747	-0.01607	-0.01975	-0.01417
F7-C6-C4-N12	178.6(2)	-179.99974	-179.98938	-179.98899	-179.99046
F7-C6-N11-C2	-179.29(19)	-180.00000	179.99239	179.99183	179.99312
N11-C2-C3-N12	-1.0(3)	-0.00041	0.011336	0.01331	0.01132
N12-C4-C6-N11	-0.9(4)	-0.00115	0.01162	0.01265	0.01134

Table 4.2 The calculated and experimental geometrical bond parameters of the ribavirin

Ribavirin	Exp. (Prusiner and Sundaralingam 1976)	B3LYP 6-311G (d, p) Gas	B3LYP 6-311G (d, p) Water	B3LYP 6-311+G (d, p) Gas	B3LYP 6-311+G (d, p) Water
Bond lengths (Å)					
C8-N24	1.328(26)	1.36381	1.35162	1.36444	1.35021
C8-O29	1.235(6)	1.21384	1.22444	1.21534	1.22796
C8-C3	1.487(6)	1.50099	1.49764	1.50064	1.49682
C3-N22	1.321(5)	1.33010	1.32815	1.33018	1.32798
C3-N23	1.361(5)	1.35925	1.36043	1.35909	1.36009
N23-C6	1.332(6)	1.31851	1.32275	1.31880	1.32312
C6-N21	1.327(5)	1.35762	1.35349	1.35775	1.35327
N21-N22	1.368(5)	1.34767	1.34619	1.34809	1.34662
N21-C1	1.475(5)	1.46926	1.47612	1.46909	1.47638
C1-C2	1.528(5)	1.53625	1.53543	1.53805	1.53693
C2-O26	1.427(5)	1.41354	1.41670	1.41478	1.41876
C2-C4	1.523(6)	1.54157	1.54318	1.54166	1.54365
C4-O27	1.418(5)	1.42579	1.42204	1.42566	1.42195
C4-C5	1.519(6)	1.53361	1.53382	1.53479	1.53486
C5-O25	1.464(5)	1.43799	1.44705	1.43857	1.44808
O25-C1	1.393(5)	1.41063	1.40676	1.41171	1.40770
C5-C7	1.509(6)	1.51480	1.51384	1.51533	1.51437
C7-O28	1.435(6)	1.42596	1.42710	1.42849	1.42974
R^2		0.96093	0.97616	0.96164	0.97804
Bond angles (°)					
O29-C8-N24	123.8(3)	124.13255	124.18498	123.80858	123.81906
O29-C8-C3	119.4(3)	122.54437	121.56942	123.80858	121.48787
N24-C8-C3	116.7(3)	113.32237	114.24559	113.69248	114.69306
C8-C3-N22	122.3(3)	121.81831	122.37702	121.77551	122.29988
C3-N23-C6	102.1(3)	103.09570	103.04944	103.18182	103.17432
C3-N22-N21	101.6(3)	102.73616	102.80258	102.83299	102.91417

Table 4.2 The calculated and experimental geometrical bond parameters of the ribavirin (Continued)

Ribavirin	**Exp. (Prusiner and Sundaralingam 1976)**	**B3LYP 6-311G (d, p) Gas**	**B3LYP 6- 311G (d, p) Water**	**B3LYP 6-311+G (d, p) Gas**	**B3LYP 6-311+G (d, p) Water**
N21-C6-N23	110.5(3)	110.02002	109.84762	109.99986	109.79137
N22-N21-C6	110.3(3)	109.63482	109.87368	109.57571	109.82925
N22-N21- C1	118.9(3)	120.25670	120.53784	120.26837	120.50632
N21-C1-C2	111.4(3)	112.55575	112.66967	112.70610	112.76193
N21-C1-O25	107.9(3)	108.46941	108.35967	108.42911	108.40524
C1-C2-O26	106.0(3)	107.93743	107.75896	107.80554	107.70471
O25-C1-C2	107.7(3)	107.09433	107.37027	107.11908	107.38078
C1-O25-C5	109.7(3)	111.13997	111.23821	111.30815	111.46322
O25-C5-C7	108.3(3)	109.86900	109.88837	109.83891	109.87984
C1-C2-C4	101.3(3)	102.00050	102.26764	102.09996	102.36273
C2-C4-C5	101.6(3)	101.90290	102.36436	102.12309	102.63861
C4-C2-O26	111.6(3)	109.79810	109.76051	110.56497	110.54143
O25-C5-C4	104.0(3)	105.26700	105.34611	105.00560	105.09841
C4-C5-C7	117.7(3)	115.46118	115.62490	115.74001	115.98572
O27-C4-C2	109.7(3)	112.20228	112.02701	112.20063	112.20124
C5-C4-O27	113.6(3)	109.42017	109.15816	110.15240	109.73404
C5-C7-O28	110.2(3)	109.12410	109.30841	109.32404	109.56838
R^2		0.92582	0.93551	0.92949	0.94673
Torsion angles (°)					
O29-C8-C3-N23		1.33943	0.16813	2.05386	0.01366
O29-C8-C3-N22		-178.93396	179.76013	-178.29712	179.49105
N24-C8-C3-N23		-178.95464	-179.85938	-178.18457	179.97959
C8-C3-N23-C6		179.80934	179.71391	179.74064	179.63714
C8-C3-N22-N21		-179.81877	-179.74134	-179.69362	-179.61670
C3-N23-C6-N21		-0.03175	-0.02688	-0.09424	-0.09537
C3-N22-N21-C6		0.04497	0.09324	-0.04664	0.02987
C3-N22-N21-C1		-178.78626	-179.66036	-178.10490	-179.13077
N23-C6-N21-C1		178.67200	179.68168	177.90027	179.10480
N22-N21-C1-C2		81.28984	83.66754	83.95952	86.72049
C6-N21-C1-C2		-97.27107	-96.03177	-93.64800	-92.25388
N21-C1-C2-O26		-150.74473	-150.15345	-148.60457	-148.05112
N21-C1-O25-C5		-116.06246	-115.49843	-117.69418	-116.75197
C1-C2-C4-O27		151.14595	149.62346	151.61174	149.95212
C1-O25-C5-C4		16.96322	15.21412	18.00265	15.85963
C1-C2-C4-C5		34.20698	32.80844	33.69074	32.22495
O26-C2-C4-O27		36.86826	35.43202	37.12695	35.45805
O26-C2-C4-C5		-80.07071	-81.38301	-80.79405	-82.26912
O25-C5-C4-O27		-150.91983	-148.85889	-151.60451	-149.42875
O25-C5-C7-O28		-68.71909	-66.62492	-68.24472	-65.59006
C1-O25-C5-C7		141.88599	140.39735	143.08124	141.31902
C4-C5-C7-O28		50.10832	52.43062	50.40912	53.38221
O27-C4-C5-C7		87.73685	89.61538	87.11028	89.01597

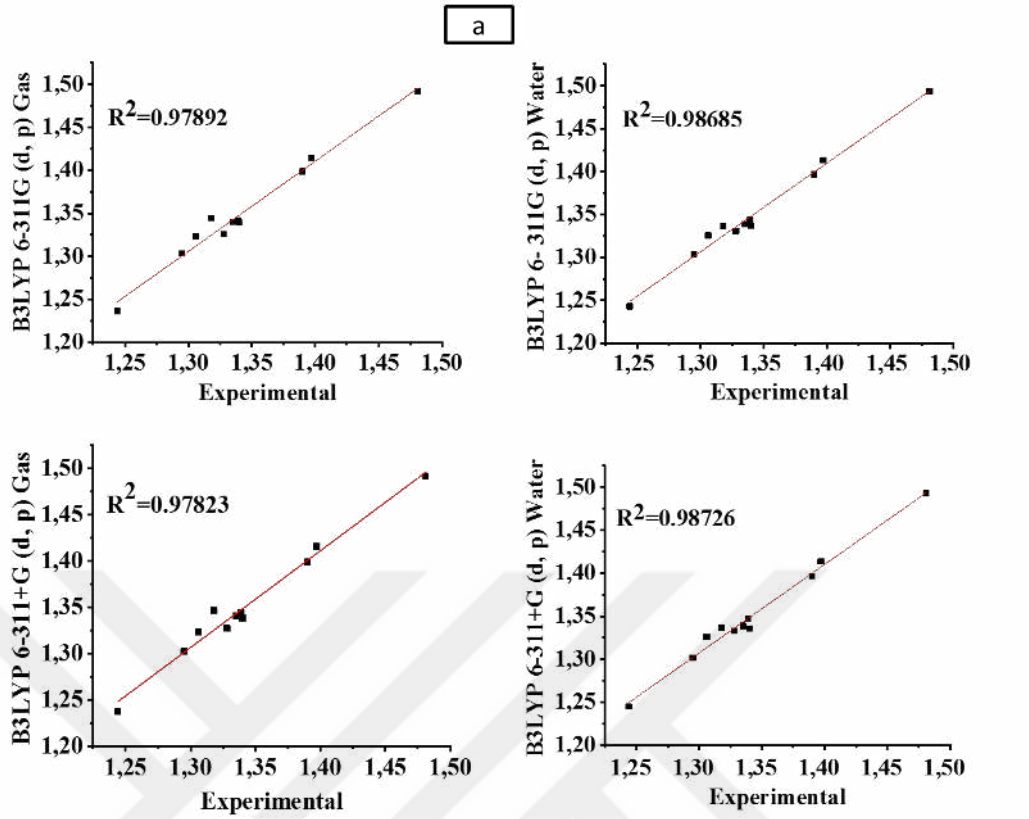

Figure 4.5 Comparison of bond lengths of favipiravir

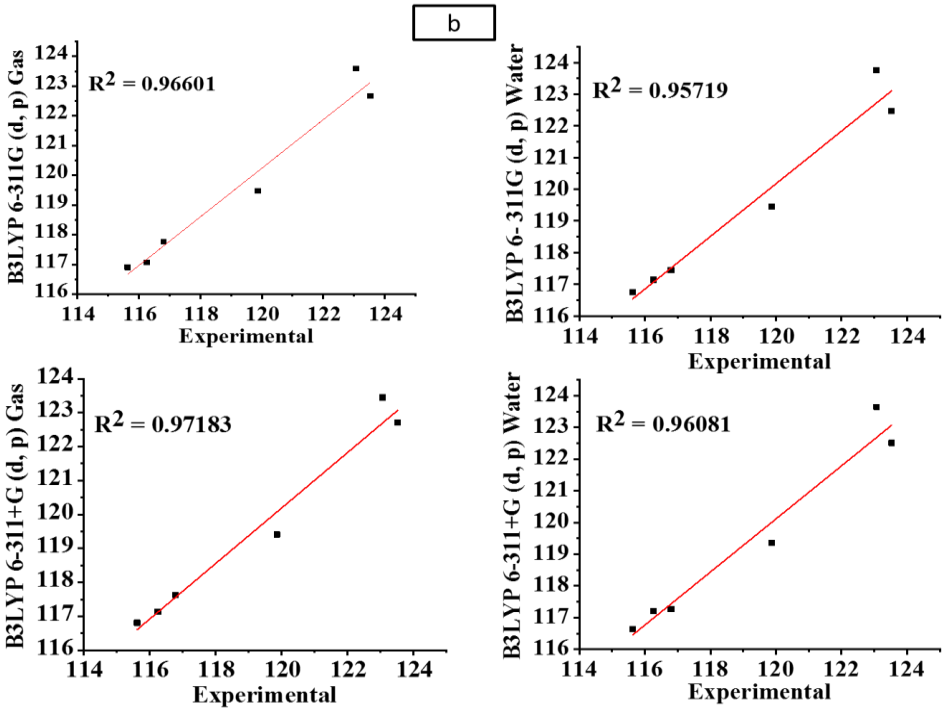

Figure 4.6 Comparison of bond angles of favipiravir

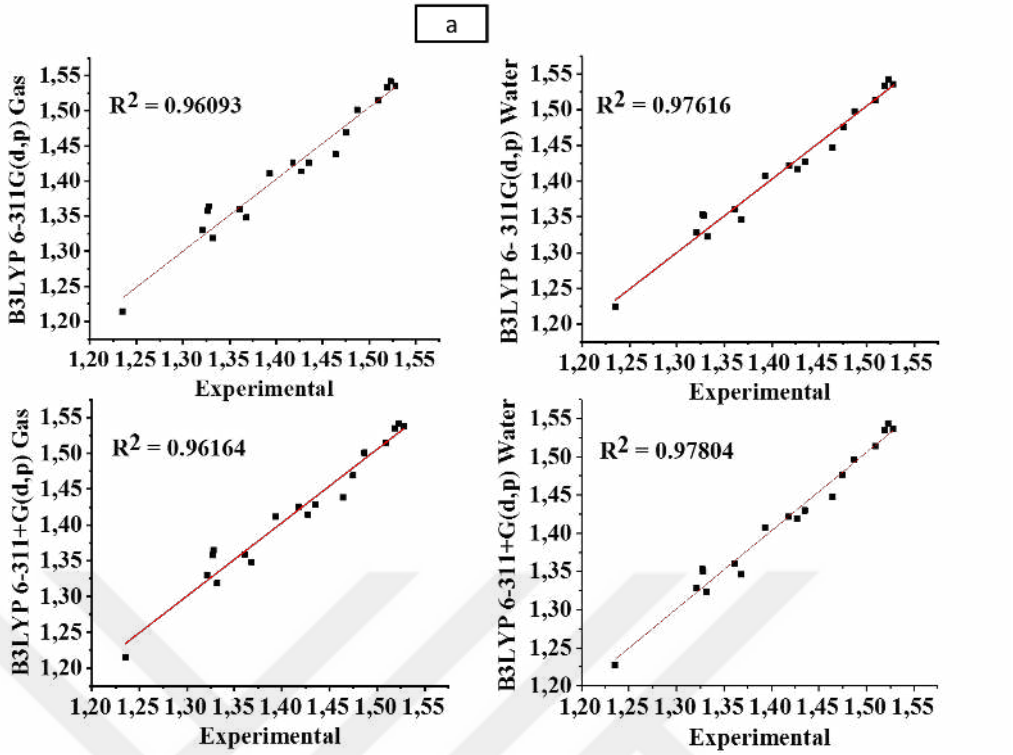

Figure 4.7 Comparison of bond lengths of ribavirin

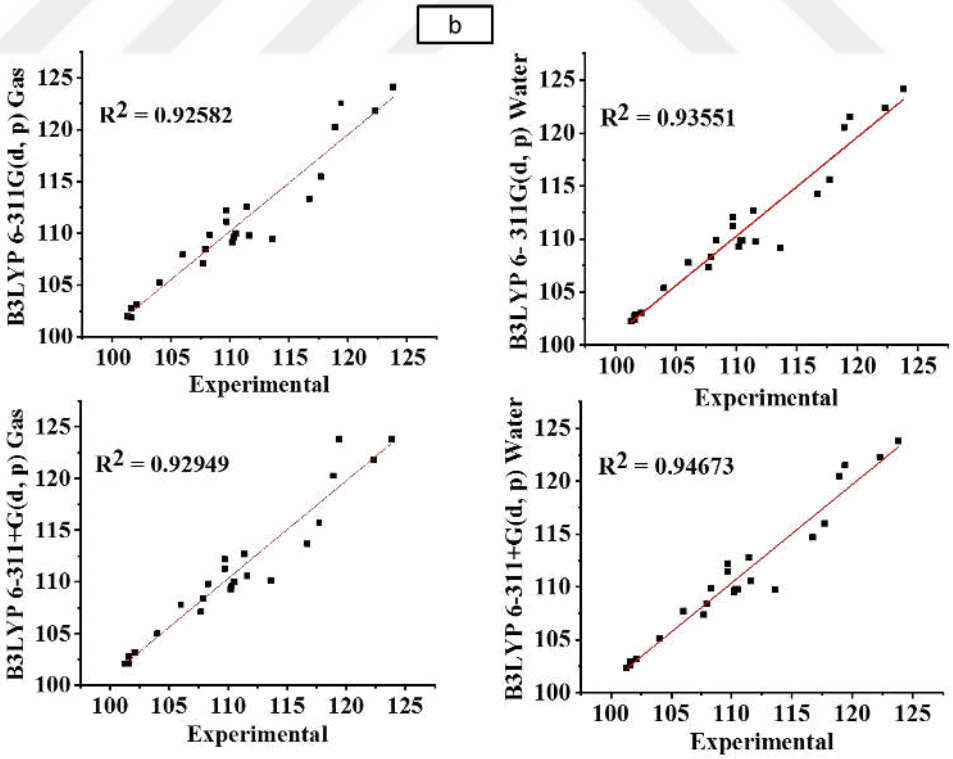

Figure 4.8 Comparison of bond angles of ribavirin

4.2 The Energy Studies of the Favipiravir and Ribavirin Molecular Structures

The ground state B3LYP/6-311G(d, p) and B3LYP/6-311+G(d, p) methods were used to compute the molecular orbital energy values, total energy, and dipole moment of the favipiravir and ribavirin compounds in both gas and water environments by a single point energy calculation. The lowest molecular orbital, LUMO, which is not occupied by any electrons, and the highest molecular orbital, HOMO, which is filled with electrons from molecular orbitals made of a linear combination of atomic orbitals, are both crucial energy levels for comprehending the chemical activity of a molecule.

Frontier molecular orbitals are the name given to these orbitals. A molecule's molecular structure becomes softer and more unstable as its HOMO-LUMO energy gap narrows; conversely, a molecule's molecular structure becomes harder and more stable as its HOMO-LUMO gap widens. Soft molecules are therefore more reactive and unstable chemically. When given enough energy, donor electrons at the HOMO level of a molecule can move to the acceptor LUMO level of metal ions.

Molecule stability metrics include the HOMO-LUMO gap and total energy of the molecule. A molecule structure with a big total energy and a small HOMO-LUMO gap is unstable and may transmit electrons readily. A molecule structure is considered stable if it has a large HOMO-LUMO gap and a low total energy (Demir Kanmazalp *et al.* 2017, Demir Kanmazalp *et al.* 2018 Kanmazalp *et al.* 2019, Demircioğlu *et al.* 2015, Zülfikaroğlu *et al.* 2018, Zülfikaroğlu 2020, Zülfikaroğlu 2021).

Additionally, the donor qualities will be better the lower the values of chemical potential (μ), chemical hardness (η), and global electrophilicity index (ω) from the global reactivity parameters of the molecular structure.

The computed dipole moments, molecular orbital energy values, and energy ranges for the favipiravir and ribavirin molecular structures are shown in Table 4.3 and Table 4.4.

Table 4.3 The calculated frontier orbital energies, the total energies, and HOMO-LUMO energy gaps (ΔE) of favipiravir by the DFT method

Favipiravir	E_{HOMO} **(eV)**	E_{LUMO} **(eV)**	μ (D)	**Total Energy (a.u.)**	ΔE **(eV)**
B3LYP/6-311G (d, p) Gas	-7.110663196	-2.566598112	3.245644	-607.672297	4.544065084
B3LYP/6-311G(d, p) Water	-7.081274668	-2.4898614	4.380018	-607.683266	4.591413268
B3LYP/6-311+G (d, p) Gas	-7.366724352	-2.848510288	3.243045	-607.689531	4.518214064
B3LYP/6-311+G (d, p) Water	-7.317471356	-2.741840816	4.548473	-607.701975	4.57563054

Table 4.4 The calculated frontier orbital energies, the total energies, and HOMO-LUMO energy gaps (ΔE) of ribavirin by the DFT method

Ribavirin	E_{HOMO} **(eV)**	E_{LUMO} **(eV)**	μ (D)	**Total Energy (a.u.)**	ΔE **(eV)**
B3LYP/6-311G (d, p) Gas	-6.7824913	-0.710766992	7.576453	-907.421923	6.071724308
B3LYP/6-311G (d, p) Water	-7.448087036	-1.11159386	9.540988	-907.449228	6.336493176
B3LYP/6-311+G (d, p) Gas	-7.099778556	-1.059075472	7.756421	-907.449932	6.040703084
B3LYP/6-311+G (d, p) Water	-7.739251156	-1.46126292	9.909418	-907.479462	6.277988236

The overall energy of the molecular structure formed in the aqueous environment is the lowest and the energy range is the broadest, according to the calculation findings. It is given the molecular orbital energies for favipiravir and ribavirin in Figure 4.9 and Figure 4.10. Energy calculations for favipiravir and ribavirin compounds are available in the literature with similar methods. The energy values were compared and the results were found to be slightly different (Hagar *et al.* 2020, Soliman and Aal 2021). Since the calculations made in this thesis study were made in the water environment, the results varied.

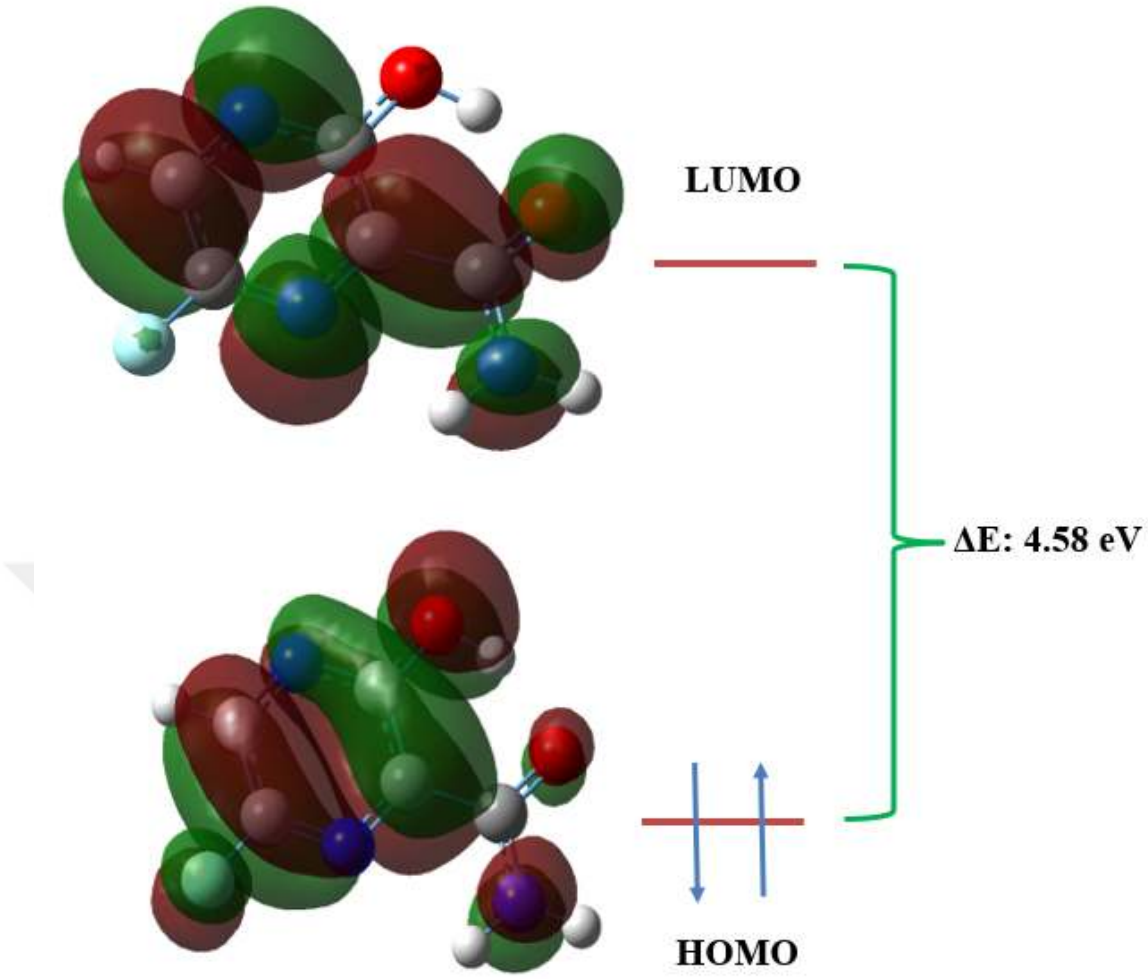

Figure 4.9 The molecular orbital energies of the molecular structure of favipiravir in a water medium by using B3LYP/6-311+G(d, p)

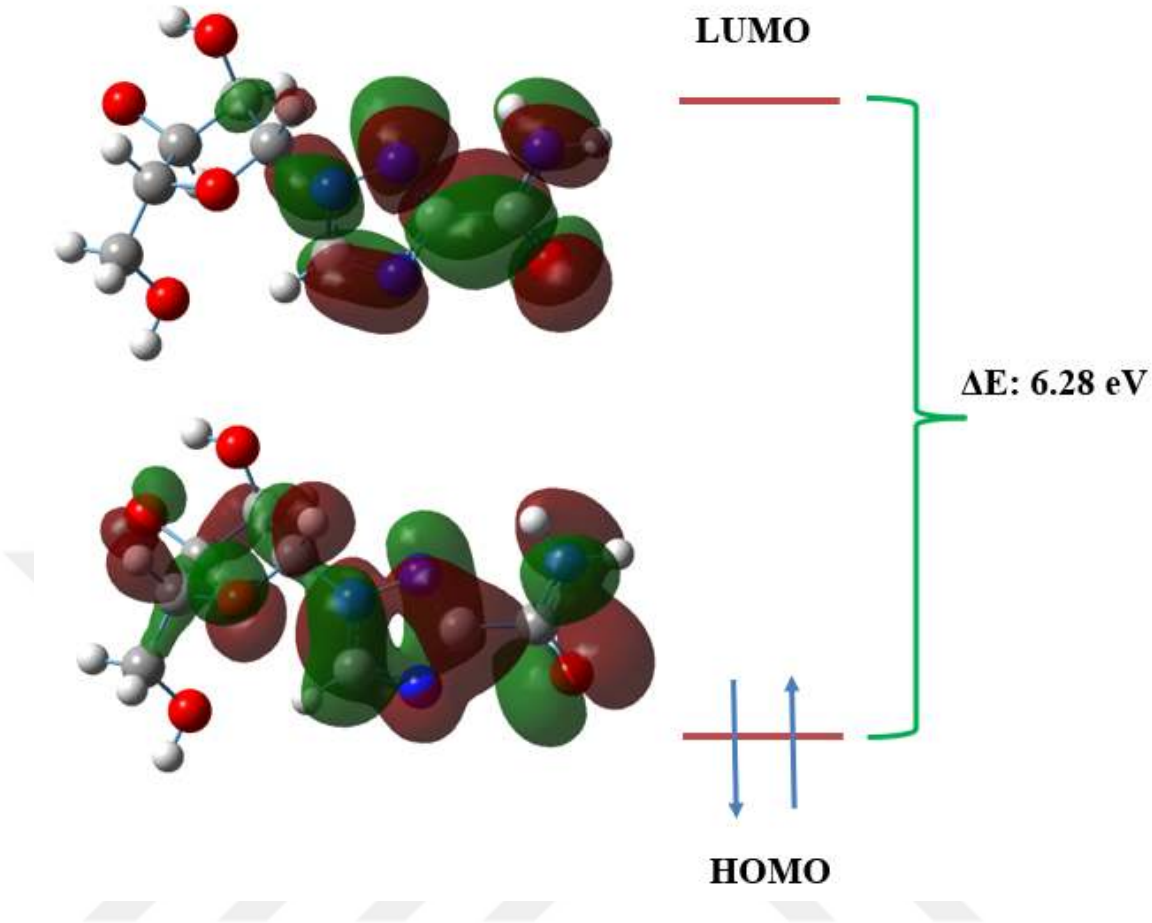

Figure 4.10 The molecular orbital energies of the molecular structure of ribavirin in a water medium by using B3LYP/6-311+G(d, p)

4.3 Interaction Studies of Favipiravir and Ribavirin Molecular Structures with DNA Bases

Molecular orbital energy values of the molecular structures of favipiravir and ribavirin were used to determine global reactivity characteristics. The least amount of power necessary to take one electron from a molecule is referred to as the ionization potential (IP). When a molecule receives an additional electron, it gains energy, which is known as electron affinity (EA). An atom's capacity to draw electrons to a molecule is known as electronegativity (χ). The electronegativity's negative value (-χ) corresponds to the chemical potential (μ). The amount to which charge transfer inside the molecule is suppressed is measured by chemical hardness (η). Chemically tough molecules either have a little intracellular charge or very little of it (Pearson 1997).

These parameters of the molecule are defined as Equation (4.1), Equation (4.2), Equation (4.3), Equation (4.4), Equation (4.5).

$$IP = -E_{HOMO} \tag{4.1}$$

$$EA = -E_{LUMO} \tag{4.2}$$

$$\chi = \frac{(IP+EA)}{2} \tag{4.3}$$

$$\mu = -\chi \tag{4.4}$$

$$\eta = \frac{(IP-EA)}{2} \tag{4.5}$$

where E_{LUMO} represents the lowest vacant molecular orbital energy and E_{HOMO} represents the highest busy molecular orbital energy in Equation (4.1) and Equation (4.2).

The electrophilicity index (ω) and global softness (*S*) are defined as follows Equation (4.6), Equation (4.7);

$$\omega = \frac{\mu^2}{2\eta} \tag{4.6}$$

$$S = \frac{1}{2\eta} \tag{4.7}$$

In the thesis study, the interaction between DNA bases and molecular structure is studied using the ECT (electrophilicity-based charge transfer) approach and ΔN (charge transfer) parameters. Following are the ΔN and ECT formulae. The fractional number of electrons is represented by the ΔN variable, which is sent between systems A to B. This parameter is used to look at the overall interactions between the DNA bases and the molecular structure as in Equation (4.8).

$$\Delta N = \frac{\mu_B - \mu_A}{2(\eta_A + \eta_B)} \quad (4.8)$$

Chemical hardnesses and potentials of two systems, A and B, are denoted here as μA, μB and ηA, ηB, respectively. A serves as an electron donor in the case where ΔN<0, while B receives the charge in the case when ΔN>0. ΔNmax is the maximal electronic charge as in Equation (4.9).

$$\Delta N_{max} = -\mu/\eta \quad (4.9)$$

In terms of ΔN_{max}, the electrophilicity index of a system may be expressed as follows Equation (4.10).

$$\omega = \frac{\mu^2}{2\eta} = \left(-\frac{\mu}{2}\right)\left(-\frac{\mu}{\eta}\right) = \chi \Delta N_{max}/2 \quad (4.10)$$

so, Equation (4.11);

$$\Delta N_{max} = \frac{2\omega}{\chi} = 2\omega X \quad (4.11)$$

where, $X = 1/\chi$

When two systems, such as A and B, are close to one another, the electrophilicity, or electrophilicity-based charge transfer (ECT), of the amount of charge transfer between them which can be represented as follows Equation (4.12).

$$ECT = (\Delta N_{max})_A - (\Delta N_{max})_B = 2[\omega_A X_A - \omega_B X_B] \quad (4.12)$$

If (ECT) is less than zero, the charge moves from A to B (where A serves as an electron donor), and vice versa if (ECT) is greater than zero, the charge moves from B to A and serves as an electron acceptor. One system that uses a constant chemical potential must

be formed when two systems, say X and Y, are united, much like in a reaction. Negative chemical potential is frequently referred to as absolute electronegativity since a less electronegative system will always give up electrons to a more electronegative one (Parr 1980, Iczkowski and Margrave 1961). To better understand how favipiravir and ribavirin molecular structures and DNA bases interact, this work employed the ΔN and ECT techniques to measure charge transfer rates between DNA bases and the molecular structures of favipiravir and ribavirin. The global reactivity parameters obtained from the HOMO and LUMO energy values of the molecular structures of favipiravir and ribavirin are given in Table 4.5 and Table 4.6. The optimized molecular geometry of DNA bases is given in Figure 4.11. In Table 4.7 and Table 4.8, the global reactivity parameters with ΔN and ECT parameters (B: Molecule, A: DNA bases) obtained by using DFT/B3LYP/6-311+G(d, p) in the water medium of favipiravir, ribavirin, and DNA bases are given (Çınarlı *et al.* 2020). Since the lowest energy molecular structures were obtained by the 6-311+G(d, p) method, global reactivity parameters obtained from this method were used in ΔN and ECT calculations.

Table 4.5 The global reactivity parameters of the molecular structures of favipiravir

Favipiravir	**B3LYP/6-311G (d, p) Gas**	**B3LYP/6- 311G (d, p) Water**	**B3LYP/6-311+G (d, p) Gas**	**B3LYP/6-311+G (d, p) Water**
IP (eV)	7.110663196	7.081274668	7.366724352	7.317471356
EA (eV)	2.566598112	2.4898614	2.848510288	2.741840816
χ (eV)	4.838630654	4.785568034	5.10761732	5.029656086
μ (eV)	-4.838630654	-4.785568034	-5.10761732	-5.029656086
η (eV)	2.272032542	2.295706634	2.259107032	2.28781527
S (eV)	0.220067270	0.217797863	0.221326388	0.218549113
ω (eV)	5.152291213	4.987932924	5.773908521	5.528733170

Table 4.6 The global reactivity parameters of the molecular structures of ribavirin

Ribavirin	**B3LYP/6-311G (d, p) Gas**	**B3LYP/6-311G (d, p) Water**	**B3LYP/6-311+G (d, p) Gas**	**B3LYP/6-311+G (d, p) Water**
IP (eV)	6.7824913	7.448087036	7.099778556	7.739251156
EA (eV)	0.710766992	1.11159386	1.059075472	1.46126292
χ (eV)	3.746629146	4.279840448	4.079427014	4.600257038
μ (eV)	-3.746629146	-4.279840448	-4.079427014	-4.600257038
η (eV)	3.035862154	3.168246588	3.020351542	3.138994118
S (eV)	0.164697859	0.157815998	0.165543643	0.159286695
ω (eV)	2.311901734	2.890721058	2.754931757	3.370883158

Table 4.7 The global reactivity parameters with ΔN and ECT parameters (B: Molecule, A: DNA bases) were obtained by using DFT/B3LYP/6-311+G(d, p) in a water medium of favipiravir and DNA bases

	Adenine	**Guanine**	**Cytosine**	**Thymine**	**Favipiravir**
E_{HOMO} **(eV)**	-6.239	-5.873	-6.556	-6.819	-7.317
E_{LUMO} **(eV)**	-0.809	-0.420	-0.998	-1.133	-2.742
Total Energy (a.u.)	-467.45	-542.72	-395.06	-453.59	-607.70
IP (eV)	6.239	5.873	6.552	6.819	7.317
EA (eV)	0.809	0.420	0.998	1.133	2.742
μ **(eV)**	-3.524	-3.146	-3.775	-3.976	-5.030
χ **(eV)**	3.524	3.146	3.775	3.976	5.030
η **(eV)**	2.715	2.726	2.777	2.843	2.288
S (eV^{-1})	0.184	0.183	0.180	0.176	0.219
ω **(eV)**	2.467	1.817	2.566	2.779	5.529
ΔN	-0.150509	-0.187873	-0.123899	-0.102709	
ECT	-0.7931	-1.037506	-0.834636	-0.794426	

Table 4.8 The global reactivity parameters and ΔN and ECT parameters (B: Molecule, A: DNA bases) were obtained by using DFT/B3LYP/6-311+G(d, p) in a water medium of ribavirin and DNA bases

	Adenine	**Guanine**	**Cytosine**	**Thymine**	**Ribavirin**
E_{HOMO} **(eV)**	-6.239	-5.873	-6.556	-6.819	-7.739
E_{LUMO} **(eV)**	-0.809	-0.420	-0.998	-1.133	-1.461
Total Energy (a.u.)	-467.45	-542.72	-395.06	-453.59	-907.48
IP (eV)	6.239	5.873	6.552	6.819	7.739
EA (eV)	0.809	0.420	0.998	1.133	1.461
μ (eV)	-3.524	-3.146	-3.775	-3.976	- 4.600
χ (eV)	3.524	3.146	3.775	3.976	4.600
η (eV)	2.715	2.726	2.777	2.843	3.139
S (eV^{-1})	0.184	0.183	0.180	0.176	0.159
ω (eV)	2.467	1.817	2.566	2.779	3.371
ΔN	-0.091902	-0.123955	-0.069726	-0.052156	
ECT	-0.066692	-0.311036	-0.108166	-0.067956	

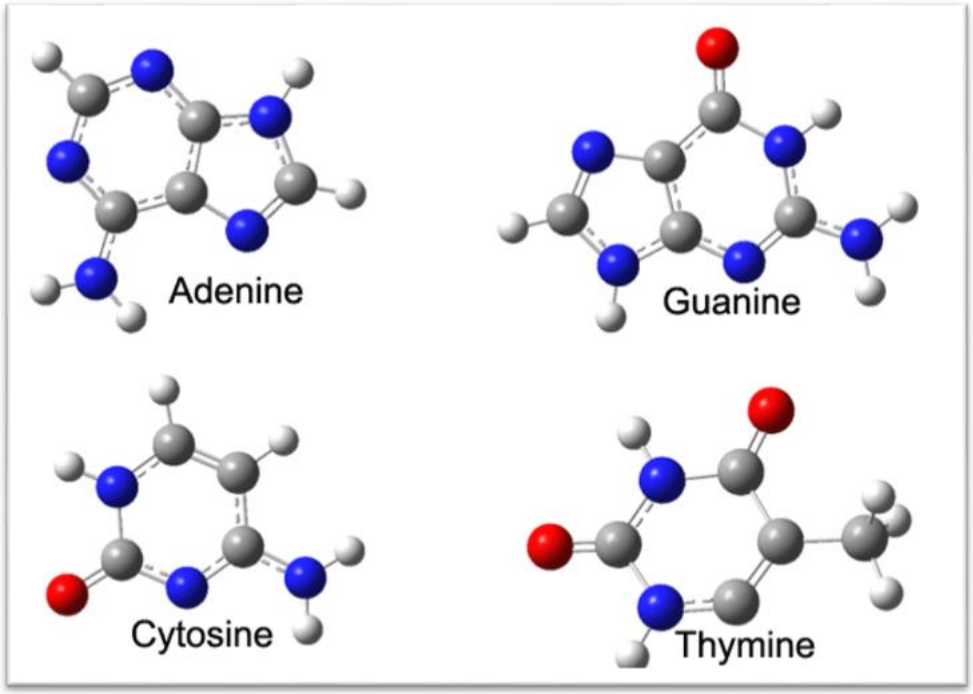

Figure 4.11 DFT/B3LYP/6-311+G (d, p) analysis of the molecular morphologies of the DNA bases in the aqueous phase

Molecular electrostatic potential (MEP) maps of favipiravir and ribavirin molecular structures with guanine bases can be seen in Figure 4.12 and Figure 4.13. Their Molecular Electrostatic Potential (MEP) maps are obtained by using B3LYP/6-311+G(d, p).

We may conclude that ECT therapy leads to more reliable outcomes when compared to ΔN. Lower electrophilicity indices are seen in more nucleophilic compounds than in electrophilic ones. According to this, the DNA nucleotide guanine has the lowest electrophilicity index. The ECT data also suggests the guanine base and the molecule structure interact primarily.

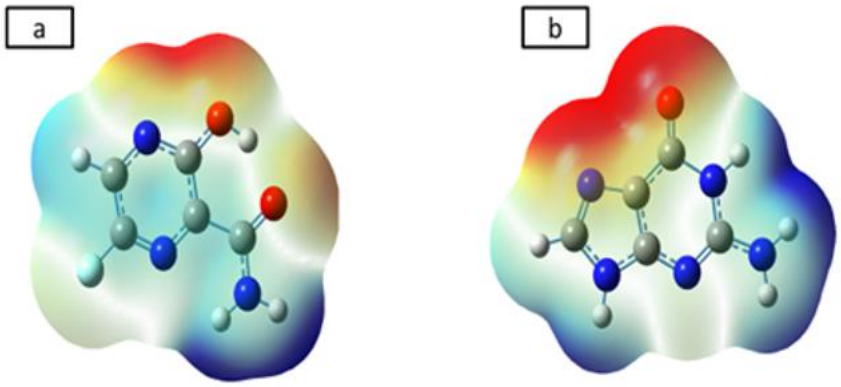

Figure 4.12 Molecular electrostatic potential maps of a) favipiravir and b) guanine base

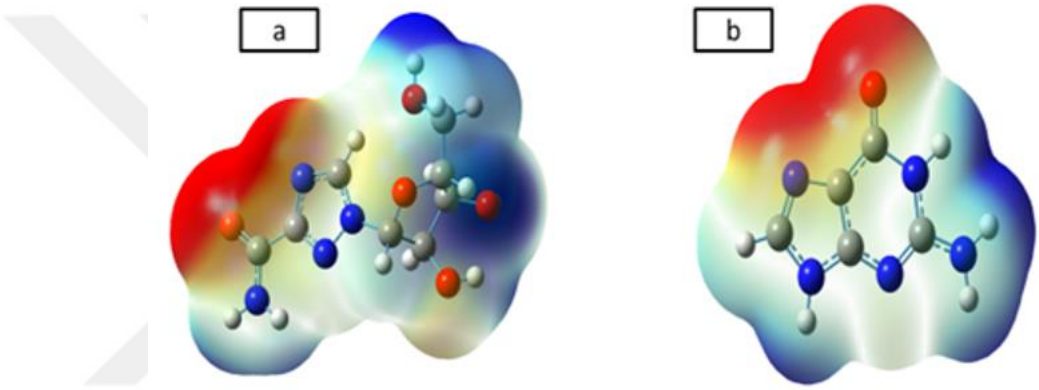

Figure 4.13 Molecular electrostatic potential maps of a) ribavirin and b) guanine base

A molecule's MEP surface reveals the locations of its chemically active areas. Understanding the nucleophilic and electrophilic areas of the molecule as well as defining interactions inside and between molecules is crucial. On the surface of potential energy, blue regions define regions that are more electrophilic, and red define regions that are more nucleophilic.

It can be said that the electrophilic region of favipiravir is concentrated in the NH_2 group, the electrophilic region of ribavirin is concentrated in the OH group, and the guanine base is concentrated in the N and O atoms of the nucleophilic region.

4.4 Thermodynamic Properties of Favipiravir and Ribavirin Molecular Structures

In the thesis study, using B3LYP/6-311G(d, p) and B3LYP/6-311+G(d, p) levels in gas and water media, we calculated total energy, dipole moment, zero point vibrational (ZPVE) energy, and the standard thermodynamic parameters such as standard heat capacity C_{vib}, standard entropy S_{vib}, standard enthalpy H_{vib}, and Gibbs free energies of the favipiravir, ribavirin compounds, and guanine base at 298.15 K temperature and 1 atm pressure. As shown in Table 4.9 and Table 4.10, the ZPVE and E_{total} values of the favipiravir, ribavirin molecular structure produced using the B3LYP/6-311+G(d, p) technique in the water phase are significantly lower than those obtained using the B3LYP/6-311G(d, p) method.

Table 4.9 The calculated thermodynamic parameters of favipiravir compound and guanine base using B3LYP/6-311G(d, p), B3LYP/6-311+G(d, p) methods

Favipiravir					
Thermodynamic parameters	**B3LYP/6-311G(d, p) Gas**	**B3LYP/6-311G (d, p) Water**	**B3LYP/6-311+G(d, p) Gas**	**B3LYP/6-311+G(d, p) Water**	**Guanine B3LYP/6-311+G(d, p) Water**
SCF energy (Hartree)	-607.6722	-607.6832	-607.6895	-607.7019	-542.7224
Total energy (thermal), E_{total} (kcal mol^{-1})	68.558	68.255	68.350	68.042	77.579
Heat capacity at const. volume, C_{vib} (cal mol^{-1} K^{-1})	33.217	33.301	33.416	33.483	31.240
Entropy, S_{vib} (cal mol^{-1} K^{-1})	91.629	91.768	91.962	92.086	87.524
Enthalpy, H (kcal mol^{-1})	6.029738	6.043543	6.069899	6.079939	5.5333
Gibbs Free Energy(kcal mol^{-1})	41.8316	41.4871	41.5235	41.1784	52.0757
The vibrational energy, E_{vib} (kcal mol^{-1})	66.781	66.478	66.572	66.264	75.801
The zero-point vibrational energy, E_0 (kcal mol^{-1})	63.12106	62.80401	62.87270	62.55417	72.63794
Rotational constants (GHz)					
A	1.83438	1.84095	1.83032	1.83730	1.92633
B	0.95957	0.95717	0.95923	0.95673	1.11603
C	0.63001	0.62975	0.62939	0.62913	0.70664
Dipole moment (Debye)	3.2457	4.3800	3.2430	4.5485	9.1968

Table 4.10 The calculated thermodynamic parameters of ribavirin compound and guanine base using B3LYP/6-311G(d, p), B3LYP/6-311+G(d, p) methods

Ribavirin					
Thermodynamic parameters	**B3LYP/6-311G(d, p) Gas**	**B3LYP/6-311G (d, p) Water**	**B3LYP/6-311+G(d, p) Gas**	**B3LYP/6-311+G(d, p) Water**	**Guanine B3LYP/6-311+G(d, p) Water**
SCF energy (Hartree)	-907.4219	-907.4492	-907.4499	-907.4794	-542.7224
Total energy (thermal), E_{total} (kcal mol^{-1})	151.614	151.483	151.318	151.185	77.579
Heat capacity at const. volume, C_{vib}(cal mol^{-1} K^{-1})	60.148	60.079	60.539	60.470	31.240
Entropy, S_{vib} (cal mol^{-1} K^{-1})	130.354	129.395	132.126	130.664	87.524
Enthalpy, H (kcal mol^{-1})	10.788770	10.729784	10.915527	10.843991	5.5333
Gibbs Free Energy (kcal mol^{-1})	113.3413	113.4957	112.5174	112.8199	52.0757
The vibrational energy, E_{vib} (kcal mol^{-1})	149.837	149.705	149.541	149.408	75.801
The zero-point vibrational energy, E_0 (kcal mol^{-1})	141.41819	141.34553	140.99500	140.93383	72.63794
Rotational constants (GHz)					
A	0.93435	0.93753	0.93695	0.93906	1.92633
B	0.26039	0.26002	0.25764	0.25754	1.11603
C	0.22441	0.22337	0.22237	0.22142	0.70664
Dipole moment (Debye)	7.5764	9.5410	7.7564	9.9094	9.1968

The findings from the energies, dipole moment, enthalpy, entropy, heat capacity, Gibbs free energy, and ZPVE results are useful for understanding how to research the compounds mentioned in the title. In thermochemical fields, they can be used to estimate the directions of chemical processes by the second law of thermodynamics and compute other thermodynamic energies based on correlations between thermodynamic functions.

5. CONCLUSIONS AND RECOMMENDATION

5.1 Conclusions

- It was found that the bond parameters of the optimized molecular structures of favipiravir and ribavirin compounds obtained by the B3LYP/6-311+G(d, p) method were more compatible with the literature than the other method.
- The bond lengths of the optimized molecular structure of favipiravir are more compatible with the experimental values in the water environment, and the bond angles in the gas environment. The bond parameters of the optimized molecular structure of ribavirin are even more compatible with the experimental values in the water environment.
- The molecular structures of favipiravir and ribavirin compounds were both found to be at the lowest energy at -607.70 a.u. and -907.48 a.u, in the water environment by the 6-311+G(d, p) method, respectively.
- It can be said that these two compounds are more stable in the water environment.
- Considering the ΔN and ECT values between adenine, guanine, cytosine and thymine DNA bases, and the molecular structures of favipiravir and ribavirin, we can say that the greatest interaction in terms of magnitude in both parameters is with guanine base.
- We can say that the electrophilicity index value of the guanine base is low and the ΔN and ECT values are negative, that the guanine base is the donor (nucleophilic) and the direction of charge transfer is from guanine to the molecular structures of favipiravir and ribavirin.
- According to MEP, it can be said that the electrophilic region of favipiravir is concentrated in the NH_2 group, the electrophilic region of ribavirin is concentrated in the OH group, and the guanine base is concentrated in the N and O atoms of the nucleophilic region.
- A decrease in zero-point vibration energies and Gibbs free energies, and an increase in entropy and enthalpy values were observed as the molecular structure of favipiravir, and a decrease in zero-point vibration energies, entropy, and enthalpy values and an increase in the Gibbs free energies were observed as the molecular structure of ribavirin passed from the gas environment to the water environment.

5.2 Recommendation

- The molecular structures of favipiravir and ribavirin compounds can be calculated in different solvent environments and the bond parameters can be compared.
- Nucleophilic and electrophilic atoms can be determined by calculating the Fukui functions of the molecular structures of favipiravir and ribavirin and DNA bases in water.
- With the help of the simulation program, favipiravir and ribavirin compounds and DNA bases can be reacted to obtain Gibbs free energies of the product compounds and ΔGs can be obtained.

REFERENCES

Allam, A. E., Assaf, H. K., Hassan, H. A., Shimizu, K. and Elshaier, Y. A. 2020. An in silico perception for newly isolated flavonoids from peach fruit as privileged avenue for a countermeasure outbreak of COVID-19. RSC Advances, 10(50): 29983-29998.

Atalay, Y., Avcı, D. and Başoğlu, A. 2008. Linear and non-linear optical properties of some donor–acceptor oxadiazoles by ab initio Hartree-Fock calculations. Structural Chemistry, 19(2): 239-246.

Aytür, Y. K., Köseoğlu, B. F., Taşkıran, Ö. Ö., Ordu-Gökkaya, N. K., Delialioğlu, S. Ü., Tur, B. S. and Tıkız, C. 2020. Pulmonary rehabilitation principles in SARS-COV-2 infection (COVID-19): A guideline for the acute and subacute rehabilitation. Turkish Journal of Physical Medicine and Rehabilitation, 66(2): 104.

Babashkina, M. G., Frontera, A., Kertman, A. V., Saygideger, Y., Murugavel, S. and Safin, D. A. 2022. Favipiravir: insight into the crystal structure, Hirshfeld surface analysis and computational study. Journal of the Iranian Chemical Society, 19(1): 85-94.

Bassi, M. R., Sempere, R. N., Meyn, P., Polacek, C. and Arias, A. 2018. Extinction of Zika virus and Usutu virus by lethal mutagenesis reveals different patterns of sensitivity to three mutagenic drugs. Antimicrobial Agents and Chemotherapy, 62(9): e00380-18.

Beck, K. M. and Nielsen, P. 2022. Double-Headed 2′-Deoxynucleotides That Hybridize to DNA and RNA Targets via Normal and Reverse Watson–Crick Base Pairs. The Journal of Organic Chemistry, 87(8): 5113-5124.

Becke, A. D. and Roussel, M. R. 1989. Exchange holes in inhomogeneous systems: A coordinate-space model. Physical Review A, 39(8): 3761.

Blasie, C. A. and Berg, J. M. 2002. Structure-Based Thermodynamic Analysis of a Coupled Metal Binding− Protein Folding Reaction Involving a Zinc Finger Peptide. Biochemistry, 41(50): 15068-15073.

Caly, L., Druce, J. D., Catton, M. G., Jans, D. A. and Wagstaff, K. M. 2020. The FDA-approved drug ivermectin inhibits the replication of SARS-CoV-2 in vitro. Antiviral Research, 178: 104787.

Chowdhury, P. 2020. Repurposing the combination drug of favipiravir, hydroxychloroquine and oseltamivir as a potential inhibitor against SARS-CoV-2: A computational study. ArXiv Preprint ArXiv, 2012: 652.

Cohen, A. J., Mori-Sánchez, P. and Yang, W. 2012. Challenges for density functional theory. Chemical Reviews, 112(1): 289-320.

Cramer, C. J. 2013. Essentials of computational chemistry: theories and models. John Wiley & Sons, 624 page, New York.

Crotty, S., Cameron, C. and Andino, R. 2002. Ribavirin's antiviral mechanism of action: lethal mutagenesis?. Journal of Molecular Medicine, 80(2): 86-95.

Çınarlı, M., Ataol, Ç. Y., Çınarlı, E. and İdil, Ö. 2020. Synthesis, characterization, biological, X-ray diffraction analysis and computational chemistry studies of new 2-acetylpyridine derivative hydrazone and its Zn (II) complex. Journal of Molecular Structure, 1213: 128152.

Davin, T. J. 2009. Computational chemistry of organometallic and inorganic species. PhD. Thesis, University of Glasgow, 177 page, Glasgow.

Delang, L., Abdelnabi, R. and Neyts, J. 2018. Favipiravir as a potential countermeasure against neglected and emerging RNA viruses. Antiviral Research, 153: 85-94.

Demir Kanmazalp, S., Başaran, E., Karaküçük-Iyidoğan, A., Oruç-Emre, E. E. and Dege, N. 2017. X-ray structures and spectroscopic properties of chiral thiosemicarbazides as studied by computational calculations. Phosphorus, Sulfur, and Silicon and the Related Elements, 192(7): 856-865.

Demir Kanmazalp, S., Başaran, E., Karaküçük-Iyidoğan, A., Oruç-Emre, E. E., Şen, F. and Dege, N. 2018. Synthesis, characterization, spectroscopy, X-ray structure and gaussian hybrid computational investigation of (−)-(S)-1-[2-(benzenesulfonamido) - 3- phenylpropanoyl]- 4- [(4-methyl) phenyl] thiosemicarbazide. Phosphorus, Sulfur, and Silicon and the Related Elements, 193(10): 675-684.

Demircioğlu, Z., Kaştaş, Ç. A. and Büyükgüngör, O. 2015. Theoretical analysis (NBO, NPA, Mulliken Population Method) and molecular orbital studies (hardness, chemical potential, electrophilicity and Fukui function analysis) of (E)-2-((4-hydroxy-2-methylphenylimino) methyl)-3-methoxyphenol. Journal of Molecular Structure, 1091: 183-195.

Dykstra, C. E., Frenking, G., Kim, K. S. and Scuseria, G. E. 2005. Computing technologies, theories, and algorithms. The making of 40 years and more of theoretical and computational chemistry. Theory and Applications of Computational Chemistry: The First Forty Years, 5(1).

Fernandez, H., Banks, G. and Smith, R. 1986. Ribavirin: a clinical overview. European Journal of Epidemiology, 2(1): 1-14.

Furuta, Y., Gowen, B. B., Takahashi, K., Shiraki, K., Smee, D. F. and Barnard, D. L. 2013. Favipiravir (T-705), a novel viral RNA polymerase inhibitor. Antiviral Research, 100(2): 446-454.

Furuta, Y., Komeno, T. and Nakamura, T. 2017. Favipiravir (T-705), a broad spectrum inhibitor of viral RNA polymerase. Proceedings of the Japan Academy, Series B, 93(7): 449-463.

Furuta, Y., Takahashi, K., Shiraki, K., Sakamoto, K., Smee, D. F., Barnard, D. L. and Morrey, J. D. 2009. T-705 (favipiravir) and related compounds: Novel broad-spectrum inhibitors of RNA viral infections. Antiviral Research, 82(3): 95-102.

Ghassemi, M. and Shahidian, A. 2017. Nano and bio heat transfer and fluid flow. Elsevier Science, 160 page, Amsterdam.

Gorbalenya, A. E., Baker, S. C., Baric, R. S., de Groot, R. J., Drosten, C., Gulyaeva, A. A. and Ziebuhr, J. 2020. Severe acute respiratory syndrome-related coronavirus: The species and its viruses–a statement of the Coronavirus Study Group. BioRxiv, 20(1).

Grimme, S., Goerigk, L. and Fink, R. F. 2012. Spin-component-scaled electron correlation methods. Wiley Interdisciplinary Reviews: Computational Molecular Science, 2(6): 886-906.

Groom, C. R., Bruno, I. J., Lightfoot, M. P. and Ward, S. C. 2016. The Cambridge structural database. Acta Crystallographica Section B: Structural Science, Crystal Engineering and Materials, 72(2): 171-179.

Gunasekaran, S., Balaji, R. A., Kumeresan, S., Anand, G. and Srinivasan, S. 2008. Experimental and theoretical investigations of spectroscopic properties of N-acetyl-5-methoxytryptamine. Canadian Journal of Analytical Sciences and Spectroscopy, 53(4): 149-162.

Hagar, M., Ahmed, H. A., Aljohani, G. and Alhaddad, O. A. 2020. Investigation of some antiviral N-heterocycles as COVID 19 drug: molecular docking and DFT calculations. International Journal of Molecular Sciences, 21(11): 3922.

Hartwell, L. H., Hood, L., Goldberg, M. L., Reynolds, A. E. and Silver, L. M. 2011. Genetics: from genes to genomes. McGraw-Hill, 774 page, New York.

Hashemian, S. M., Farhadi, T. and Velayati, A. A. 2021. A review on favipiravir: the properties, function, and usefulness to treat COVID-19. Expert Review of Anti-Infective Therapy, 19(8): 1029-1037.

Helmenstine, A. M. 2020. Nitrogenous bases—Definition and structures. ThoughtCo, 21(1).

Iczkowski, R. P. and Margrave, J. L. 1961. Electronegativity. Journal of the American Chemical Society, 83(17): 3547-3551.

Iyengar, S. S. and Frisch, M. J. 2004. Effect of time-dependent basis functions and their superposition error on atom-centered density matrix propagation (ADMP): connections to wavelet theory of multiresolution analysis. The Journal of Chemical Physics, 121(11): 5061-5070.

Kanmazalp, S. D., Macit, M. and Dege, N. 2019. Hirshfeld surface, crystal structure and spectroscopic characterization of (E)-4-(diethylamino)-2-((4-phenoxyphenylimino) methyl) phenol with DFT studies. Journal of Molecular Structure, 1179: 181-191.

Kelleni, M. T. 2020. Nitazoxanide/azithromycin combination for COVID-19: A suggested new protocol for early management. Pharmacological Research, 157: 104874.

Krieger, M., Scott, M. P., Matsudaira, P. T., Lodish, H. F., Darnell, J. E., Zipursky, L. and Berk, A. 2004. Molecular cell biology. William. H. Freeman and Company, 1280 page, New York.

Kumar, Y., Singh, H. and Patel, C. N. 2020. In silico prediction of potential inhibitors for the main protease of SARS-CoV-2 using molecular docking and dynamics simulation based drug-repurposing. Journal of Infection and Public Health, 13(9): 1210-1223.

Kurt, M., Babu, P. C., Sundaraganesan, N., Cinar, M. and Karabacak, M. 2011. Molecular structure, vibrational, UV and NBO analysis of 4-chloro-7-nitrobenzofurazan by

DFT calculations. Spectrochimica Acta Part A: Molecular and Biomolecular Spectroscopy, 79(5): 1162-1170.

Lee, C., Yang, W. and Parr, R. G. 1988. Development of the Colle-Salvetti correlation-energy formula into a functional of the electron density. Physical Review B, 37(2): 785.

Lewars, E. 2011. Computational chemistry. Introduction to the theory and applications of molecular and quantum mechanics. Springer Science & Business Media, 318, Berlin.

Magdaline, J. D. and Chithambarathanu, T. 2015. FT-IR, FT-Raman spectra and NBO analysis of 5-nitro-2-furoic acid: A DFT method. Materials Today: Proceedings, 2(3): 982-986.

Nagata, T., Lefor, A. K., Hasegawa, M. and Ishii, M. 2015. Favipiravir: a new medication for the Ebola virus disease pandemic. Disaster Medicine and Public Health Preparedness, 9(1): 79-81.

Nelson, D. L. and Cox, M. M. 2022. Princípios de bioquímica de Lehninger. Artmed Editora, 1304 page, Barcelona.

Nuevo, M., Milam, S. N., Sandford, S. A., Elsila, J. E. and Dworkin, J. P. 2009. Formation of uracil from the ultraviolet photo-irradiation of pyrimidine in pure H2O ices. Astrobiology, 9(7): 683-695.

Padhi, A. K. and Tripathi, T. 2021. Targeted design of drug binding sites in the main protease of SARS-CoV-2 reveals potential signatures of adaptation. Biochemical and Biophysical Research Communications, 555: 147-153.

Parniak, M. A., Vergis, E. N. and Abram, M. E. 2006. Antiviral agents. Encyclopedia of Respiratory Medicine, 129-134.

Parr, R. G. (1980). Density functional theory of atoms and molecules. In Horizons of Quantum Chemistry: Proceedings of the Third International Congress of Quantum Chemistry Held at Kyoto. Springer Netherlands, 5-15.

Pearson, R. G. 1997. Chemical hardness. John Wiley & Sons, 195 page, New York.

Perdew, J. P. and Wang, Y. 1992. Accurate and simple analytic representation of the electron-gas correlation energy. Physical Review B, 45(23): 13244.

Perdew, J. P., Chevary, J. A., Vosko, S. H., Jackson, K. A., Pederson, M. R., Singh, D. J. and Fiolhais, C. 1992. Atoms, molecules, solids, and surfaces: Applications of the

generalized gradient approximation for exchange and correlation. Physical Review B, 46(11): 6671.

Perdew, J. P., Chevary, J. A., Vosko, S. H., Jackson, K. A., Pederson, M. R., Singh, D. J. and Fiolhais, C. 1993. Erratum: Atoms, molecules, solids, and surfaces: Applications of the generalized gradient approximation for exchange and correlation. Physical Review B, 48(7): 4978.

Prusiner, P. and Sundaralingam, M. 1976. The crystal and molecular structures of two polymorphic crystalline forms of virazole (1-β-D-ribofuranosyl-1, 2, 4-triazole-3-carboxamide). A new synthetic broad sprectrum antiviral agent. Acta Crystallographica Section B: Structural Crystallography and Crystal Chemistry, 32(2): 419-426.

Raghavachari, K. 2000. Perspective on "Density functional thermochemistry. III. The role of exact exchange". Theoretical Chemistry Accounts, 103(3): 361-363.

Rana, M. and Chowdhury, P. 2020. Ivermectin and doxycycline combination as a promising drug candidate against SARS-CoV-2 infection: a computational study. ArXiv preprint ArXiv, 2012: 00653.

Rhyman, L., Tursun, M., Abdallah, H. H., Choong, Y. S., Parlak, C., Kharkar, P. and Ramasami, P. 2018. Theoretical investigation of the derivatives of favipiravir (T-705) as potential drugs for Ebola virus. Physical Sciences Reviews, 3(9).

Rybkin, V. V. 2014. Development of direct born–oppenheimer molecular dynamics with applications to water clusters and mechanochemistry. MSc. Thesis, University of Oslo, 57 page, Oslo.

Shen, C. H. 2019. Diagnostic molecular biology. Academic Press, 472 page, Cambridge.

Sheng, J. J. and Zeng, F. 2022. Discussion of the effect of shut-in after fracturing on oil recovery. In SPE improved oil recovery conference. OnePetro, 22(4).

Skariyachan, S., Gopal, D., Chakrabarti, S., Kempanna, P., Uttarkar, A., Muddebihalkar, A. G. and Niranjan, V. 2020. Structural and molecular basis of the interaction mechanism of selected drugs towards multiple targets of SARS-CoV-2 by molecular docking and dynamic simulation studies-deciphering the scope of repurposed drugs. Computers in Biology and Medicine, 126: 104054.

Snell, N. J. 2001. Ribavirin-current status of a broad spectrum antiviral agent. Expert Opinion on Pharmacotherapy, 2(8): 1317-1324.

Soliman, K. A. and Aal, S. A. 2021. Theoretical investigation of favipiravir antiviral drug based on fullerene and boron nitride nanocages. Diamond and Related Materials, 117: 108458.

Stephens, P. J., Devlin, F. J., Chabalowski, C. F. and Frisch, M. J. 1994. Ab initio calculation of vibrational absorption and circular dichroism spectra using density functional force fields. The Journal of Physical Chemistry, 98(45): 11623-11627.

Streeter, D. G., Witkowski, J. T., Khare, G. P., Sidwell, R. W., Bauer, R. J., Robins, R. K. and Simon, L. N. 1973. Mechanism of action of 1-β-D-ribofuranosyl-1, 2, 4-triazole-3-carboxamide (Virazole), a new broad-spectrum antiviral agent. Proceedings of the National Academy of Sciences, 70(4): 1174-1178.

Szabo, A. and Ostlund, N. S. 2012. Modern quantum chemistry: introduction to advanced electronic structure theory. Courier Corporation, 468 page, Massachusetts.

Tao, J., Perdew, J. P., Staroverov, V. N. and Scuseria, G. E. 2003. Climbing the density functional ladder: Nonempirical meta–generalized gradient approximation designed for molecules and solids. Physical Review Letters, 91(14): 146401.

Tyminska, N. 2013. Modern computational chemistry methods for prediction of ground- and excited-state properties in open-shell systems. PhD. Thesis, Michigan Tecnology University, 172 page, Michigan.

Uzunova, K., Filipova, E., Pavlova, V. and Vekov, T. 2020. Insights into antiviral mechanisms of remdesivir, lopinavir/ritonavir and chloroquine/hydroxy chloroquine affecting the new SARS-CoV-2. Biomedicine & Pharmacotherapy, 131: 110668.

Vosko, S. H., Wilk, L. and Nusair, M. 1980. Accurate spin-dependent electron liquid correlation energies for local spin density calculations: a critical analysis. Canadian Journal of Physics, 58(8): 1200-1211.

Wang, B., Guo, H., Ling, L., Ji, J., Niu, J. and Gu, Y. 2020. The chronic adverse effect of chloroquine on kidney in rats through an autophagy dependent and independent pathways. Nephron, 144(2): 96-108.

Wang, L., He, W., Yu, X., Hu, D., Bao, M., Liu, H. and Jiang, H. 2020. Coronavirus disease 2019 in elderly patients: characteristics and prognostic factors based on 4-week follow-up. Journal of Infection, 80(6): 639-645.

Zhang, R. and Mylonakis, E. 2021. In inpatients with COVID-19, none of remdesivir, hydroxychloroquine, lopinavir, or interferon β-1a differed from standard care for in-hospital mortality. Annals of Internal Medicine, 174(2): JC17.

Zülfikaroğlu, A. 2020. The synthesis, experimental and theoretical characterization of a Pd (II) complex from diacetyl monoxime isobutyrohydrazone. Journal of Molecular Structure, 1209: 127950.

Zülfikaroğlu, A. 2021. DFT Computational Studies on Some Cobaloximes. Erzincan University Journal of Science and Technology, 13(3): 1299-1316.

Zülfikaroğlu, A., Batı, H. and Dege, N. 2018. A theoretical and experimental study on isonitrosoacetophenone nicotinoyl hydrazone: Crystal structure, spectroscopic properties, NBO, NPA and NLMO analyses and the investigation of interaction with some transition metals. Journal of Molecular Structure, 1162: 125-139.

CURRICULUM VITAE

Personal Information

Name and Surname : Mustafa Fawzi Dawood ALOBAIDI

Education

MSc	Çankırı Karatekin University Graduate School of Natural and Applied Sciences Department of Physics	2019-Present
Undergraduate	University of Baghdad College of Education for Pure Sciences Department of Physics	2014-2018